

XBP1 promotes triple-negative breast cancer by controlling the HIF1 α pathway

Xi Chen^{1,2}, Dimitrios Iliopoulos^{3,4*}, Qing Zhang^{5*}, Qianzi Tang^{6,7*}, Matthew B. Greenblatt⁸, Maria Hatziapostolou^{3,4}, Elgene Lim⁹, Wai Leong Tam¹⁰, Min Ni⁹, Yiwen Chen¹¹, Junhua Mai¹², Haifa Shen^{12,13}, Dorothy Z. Hu¹⁴, Stanley Adoro^{1,2}, Bella Hu¹⁵, Minkyung Song^{1,2}, Chen Tan^{1,2}, Melissa D. Landis¹⁶, Mauro Ferrari^{2,12}, Sandra J. Shin¹⁷, Myles Brown⁹, Jenny C. Chang^{2,16}, X. Shirley Liu¹¹ & Laurie H. Glimcher^{1,2}

Cancer cells induce a set of adaptive response pathways to survive in the face of stressors due to inadequate vascularization¹. One such adaptive pathway is the unfolded protein (UPR) or endoplasmic reticulum (ER) stress response mediated in part by the ER-localized transmembrane sensor IRE1 (ref. 2) and its substrate XBP1 (ref. 3). Previous studies report UPR activation in various human tumours^{4–6}, but the role of XBP1 in cancer progression in mammary epithelial cells is largely unknown. Triple-negative breast cancer (TNBC)—a form of breast cancer in which tumour cells do not express the genes for oestrogen receptor, progesterone receptor and HER2 (also called ERBB2 or NEU)—is a highly aggressive malignancy with limited treatment options^{7,8}. Here we report that XBP1 is activated in TNBC and has a pivotal role in the tumorigenicity and progression of this human breast cancer subtype. In breast cancer cell line models, depletion of XBP1 inhibited tumour growth and tumour relapse and reduced the CD44^{high}CD24^{low} population. Hypoxia-inducing factor 1 α (HIF1 α) is known to be hyperactivated in TNBCs^{9,10}. Genome-wide mapping of the XBP1 transcriptional regulatory network revealed that XBP1 drives TNBC tumorigenicity by assembling a transcriptional complex with HIF1 α that regulates the expression of HIF1 α targets via the recruitment of RNA polymerase II. Analysis of independent cohorts of patients with TNBC revealed a specific XBP1 gene expression signature that was highly correlated with HIF1 α and hypoxia-driven signatures and that strongly associated with poor prognosis. Our findings reveal a key function for the XBP1 branch of the UPR in TNBC and indicate that targeting this pathway may offer alternative treatment strategies for this aggressive subtype of breast cancer.

We determined UPR activation status in several breast cancer cell lines. XBP1 expression was readily detected in both luminal and basal-like breast cancer cell lines, but the level of its spliced form was higher in the latter which consist primarily of TNBC cells; XBP1 activation was also higher in primary TNBC patient samples (Fig. 1a, b). PERK but not ATF6 was also activated (Extended Data Fig. 1a), and transmission electron microscopy revealed more abundant and dilated ER in multiple TNBC cell lines (Extended Data Fig. 1b). These data reveal a state of basal ER stress in TNBC cells.

XBP1 silencing impaired soft agar colony-forming ability and invasiveness (Extended Data Fig. 1c) of multiple TNBC cell lines, indicating that XBP1 regulates TNBC anchorage-independent growth and invasiveness. We next used an orthotopic xenograft mouse model with inducible

expression of two XBP1 short hairpin RNAs (shRNAs) in MDA-MB-231 cells. Tumour growth and metastasis to lung were significantly inhibited by XBP1 shRNAs (Fig. 1c–e and Extended Data Fig. 1d–g). This was not due to altered apoptosis (caspase 3), cell proliferation (Ki67) or hyperactivation of IRE1 and other UPR branches (Fig. 1e and Extended Data Fig. 1h, i). Instead, XBP1 depletion impaired angiogenesis as demonstrated by the presence of fewer intratumoral blood vessels (CD31 staining) (Fig. 1e). Subcutaneous xenograft experiments using two other TNBC cell lines confirmed our findings (Extended Data Fig. 1j, k). Notably, XBP1 silencing in a patient-derived TNBC xenograft model (BCM-2147) significantly decreased tumour incidence (Fig. 1f and Extended Data Fig. 1l, m).

TNBC patients have the highest rate of relapse within 1–3 years despite adjuvant chemotherapy^{7,8}. To examine XBP1's effect on tumour relapse after chemotherapeutic treatment, we treated MDA-MB-231 xenograft-bearing mice with doxorubicin and XBP1 shRNA. Notably, combination treatment not only blocked tumour growth but also inhibited or delayed tumour relapse (Fig. 2a).

Tumour cells expressing CD44^{high}CD24^{low} have been shown to mediate tumour relapse in some instances^{11–13}. To test whether XBP1 targeted the CD44^{high}CD24^{low} population, we examined the mammosphere-forming ability of cells derived from treated tumours (day 20). Mammosphere formation was increased in doxorubicin-treated tumour cells, whereas tumours treated with doxorubicin plus XBP1 shRNA displayed substantially reduced mammosphere formation (Fig. 2b), a finding confirmed using another chemotherapeutic agent, paclitaxel (Extended Data Fig. 2a, b). Hypoxia activates the UPR, and XBP1 knockdown also markedly reduced mammosphere formation in hypoxic conditions (Extended Data Fig. 2b). Furthermore, CD44 expression was reduced in XBP1-depleted tumours (Extended Data Fig. 2c).

To interrogate XBP1's effect on CD44^{high}CD24^{low} cell function further, we used mammary epithelial cells (MCF10A) carrying an inducible Src oncogene (ER-Src), where v-Src is fused with the oestrogen receptor ligand-binding domain¹⁴. Tamoxifen treatment results in neoplastic transformation and gain of a CD44^{high}CD24^{low} population that has been previously associated with tumour-initiating properties¹⁵. In transformed MCF10A-ER-Src cells, XBP1 splicing was increased in the CD44^{high}CD24^{low} population (Fig. 2c), whereas XBP1 silencing reduced the CD44^{high}CD24^{low} fraction (Extended Data Fig. 2d, e) and markedly suppressed mammosphere formation (Extended Data Fig. 2f), phenotypes

¹Sandra and Edward Meyer Cancer Center of Weill Cornell Medical College, 1300 York Avenue, New York, New York 10065, USA. ²Department of Medicine, Weill Cornell Medical College, 1300 York Avenue, New York, New York 10065, USA. ³Center for Systems Biomedicine, Division of Digestive Diseases, David Geffen School of Medicine, University of California, Los Angeles, Los Angeles, California 90095, USA.

⁴Department of Cancer Immunology and AIDS, Dana-Farber Cancer Institute, Boston, Massachusetts 02115, USA. ⁵Lineberger Comprehensive Cancer Center, Department of Pathology and Laboratory Medicine, University of North Carolina at Chapel Hill, Chapel Hill, North Carolina 27599, USA. ⁶Department of Bioinformatics, School of Life Science and Technology, Tongji University, Shanghai 200092, China. ⁷Institute of Animal Genetics and Breeding, College of Animal Science and Technology, Sichuan Agricultural University, Ya'an, Sichuan 625014, China. ⁸Department of Pathology, Brigham and Women's Hospital, Boston, Massachusetts 02115, USA. ⁹Department of Medical Oncology, Dana-Farber Cancer Institute and Department of Medicine, Harvard Medical School, Boston, Massachusetts 02115, USA. ¹⁰Whitehead Institute for Biomedical Research, 9 Cambridge Center, Cambridge, Massachusetts 02142, USA. ¹¹Department of Biostatistics and Computational Biology, Dana-Farber Cancer Institute and Harvard School of Public Health, Boston, Massachusetts 02115, USA. ¹²Department of Nanomedicine, Houston Methodist Research Institute, Houston, Texas 77030, USA. ¹³Department of Cell and Developmental Biology, Weill Cornell Medical College, 1300 York Avenue, New York, New York 10065, USA. ¹⁴Endocrine Unit, Massachusetts General Hospital, Boston, Massachusetts 02114, USA.

¹⁵Division of Hematology/Oncology, Children's Hospital Boston, Boston, Massachusetts 02115, USA. ¹⁶Houston Methodist Cancer Center, Houston, Texas 77030, USA. ¹⁷Department of Pathology and Laboratory Medicine, Weill Cornell Medical College, 1300 York Avenue, New York, New York 10065, USA.
*These authors contributed equally to this work.

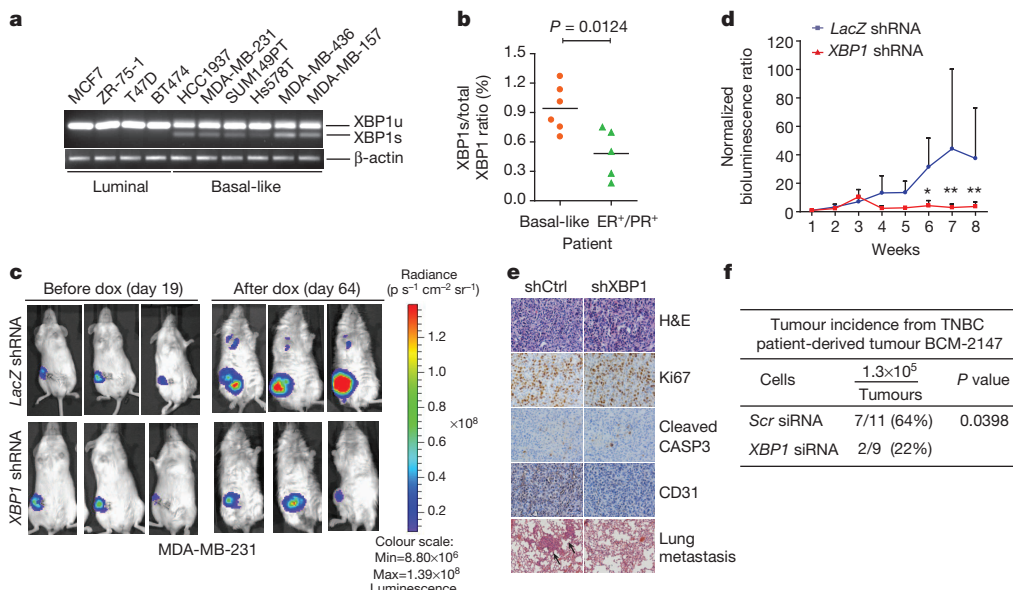


Figure 1 | XBP1 silencing blocks TNBC cell growth and invasiveness.

a, b, RT-PCR analysis of XBP1 splicing in luminal and basal-like cell lines (**a**) or primary tissues from 6 TNBC patients and 5 oestrogen/progesterone-positive (ER/PR⁺) patients (**b**). XBP1u, unspliced XBP1; XBP1s, spliced XBP1. β-actin was used as loading control. **c**, Representative bioluminescent images of orthotopic tumours formed by MDA-MB-231 cells as in Extended Data Fig. 1d. Bioluminescent images were obtained 5 days after transplantation and serially after mice were begun on chow containing doxycycline (day 19) for 8 weeks.

not attributable to a direct effect of XBP1 on cell viability (Extended Data Fig. 2g, h). Furthermore, limiting dilution experiments demonstrated loss of tumour-seeding ability in XBP1-depleted cells (Fig. 2d). CD44^{high} CD24^{low} cells sorted from TNBC patient samples confirmed increased XBP1 splicing and other UPR markers, and XBP1 silencing impaired mammosphere-forming ability (Fig. 2e, f and Extended Data Fig. 3a). Conversely, overexpression of spliced XBP1 (XBP1s) in CD44^{low}CD24^{high} cells resulted in gain of mammosphere-forming ability and increased resistance to doxorubicin treatment (Extended Data Fig. 3b, c). Notably, patient-derived CD44^{low}CD24^{high} cells overexpressing XBP1s, but not control parental cells, initiated tumour formation in immunodeficient

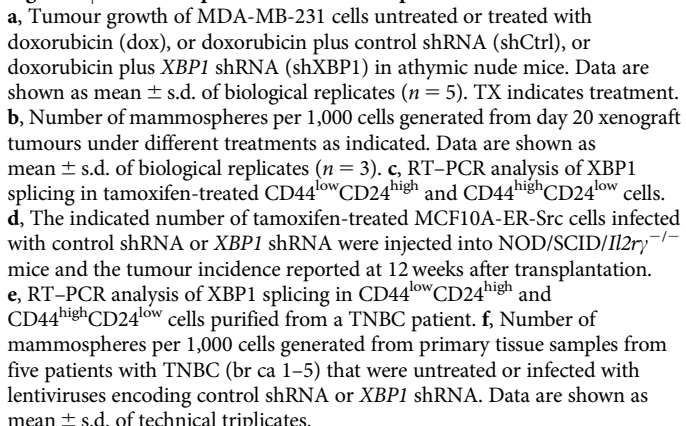
Pictures shown are the day 19 image (before dox) and day 64 image (after dox). **d**, Quantification of imaging studies as in **c**. Data are shown as mean ± s.d. of biological replicates ($n = 8$). * $P < 0.05$, ** $P < 0.01$. **e**, Haematoxylin and eosin (H&E), Ki67, cleaved caspase 3 or CD31 immunostaining of tumours or lungs 8 weeks after mice were fed chow containing doxycycline. Black arrows indicate metastatic nodules. **f**, Tumour incidence in mice transplanted with BCM-2147 tumour cells (10 weeks after transplantation). Statistical significance was determined by Barnard's test^{22,23}.

mice (Extended Data Fig. 3d, e). These data establish a critical role of XBP1 in CD44^{high}CD24^{low} cells within TNBC.

Chromatin immunoprecipitation coupled with ultra-high-throughput DNA sequencing (ChIP-seq) and motif analysis of XBP1 in MDA-MB-231 cells revealed statistically significant enrichment of both the HIF1α and XBP1 motifs (Fig. 3a and Extended Data Fig. 4a), indicating frequent co-localization of HIF1α and XBP1 to the same regulatory elements. HIF1α is hyperactivated in TNBCs, required for the maintenance of CD44^{high}CD24^{low} cells^{9,10,16,17}, and is regulated in response to micro-environmental oxygen levels. XBP1 ChIP-seq was therefore also carried out in MDA-MB-231 and Hs578T cells cultured under hypoxia and glucose deprivation conditions for 24 h. Exposure to these stressors increased XBP1 splicing, resulting in a corresponding increase in signal intensity (Extended Data Fig. 4b-f) and further enrichment of HIF1α motifs in TNBC (Fig. 3a), but interestingly not in luminal breast cancer cells (Extended Data Fig. 4g).

HIF1α motif enrichment in the XBP1 ChIP-seq data set indicated that XBP1 and HIF1α might interact within the same transcriptional complex.

Figure 2 | XBP1 is required for tumour relapse and CD44^{high}CD24^{low} cells.



a, Tumour growth of MDA-MB-231 cells untreated or treated with doxorubicin (dox), or doxorubicin plus control shRNA (shCtrl), or doxorubicin plus XBP1 shRNA (shXBP1) in athymic nude mice. Data are shown as mean ± s.d. of biological replicates ($n = 5$). TX indicates treatment.

b, Number of mammospheres per 1,000 cells generated from day 20 xenograft tumours under different treatments as indicated. Data are shown as mean ± s.d. of biological replicates ($n = 3$). **c**, RT-PCR analysis of XBP1 splicing in tamoxifen-treated CD44^{low}CD24^{high} and CD44^{high}CD24^{low} cells.

d, The indicated number of tamoxifen-treated MCF10A-ER-Src cells infected with control shRNA or XBP1 shRNA were injected into NOD/SCID/ $\text{Il2r}\gamma^{-/-}$ mice and the tumour incidence reported at 12 weeks after transplantation.

e, RT-PCR analysis of XBP1 splicing in CD44^{low}CD24^{high} and CD44^{high}CD24^{low} cells purified from a TNBC patient. **f**, Number of mammospheres per 1,000 cells generated from primary tissue samples from five patients with TNBC (br ca 1–5) that were untreated or infected with lentiviruses encoding control shRNA or XBP1 shRNA. Data are shown as mean ± s.d. of technical triplicates.

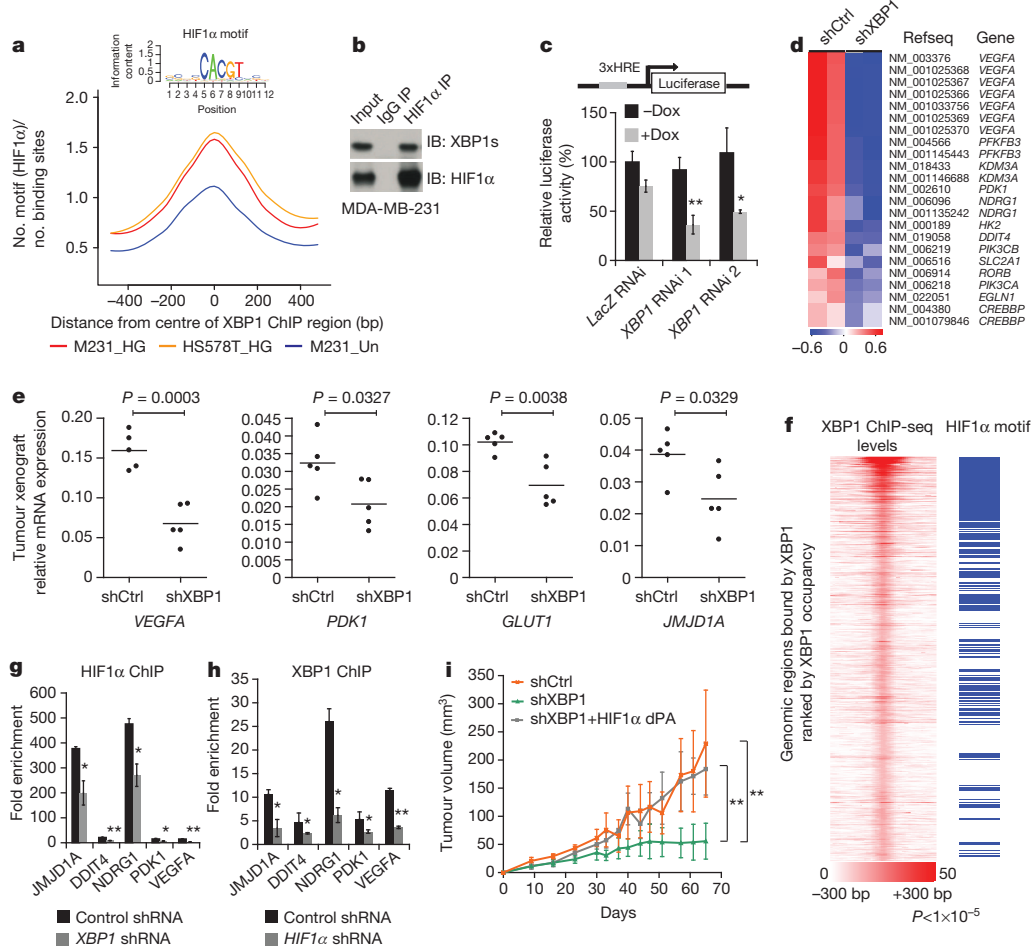


Figure 3 | HIF1 α is a co-regulator of XBP1. **a**, Motif enrichment analysis in the XBP1 binding sites in untreated (Un) or stressed (0.1% O₂ and glucose deprivation; HG) MDA-MB-231 or Hs578T cells. The 1-kilobase (kb) region surrounding the summit of the XBP1 peak is equally divided into 50 bins. The average HIF1 α motif occurrence over top 1,000 XBP1 peaks in each bin is plotted. The sequence logo for HIF1 α motif is shown as an inset. The corresponding *P* values of each condition are: M231_Un, 7.78×10^{-20} ; M231_HG, $<1.08 \times 10^{-30}$; Hs578T_HG, $<1.08 \times 10^{-30}$. **b**, Nuclear extracts from MDA-MB-231 cells (treated with 0.1% O₂ for 10 h first and then with 1 μ g ml⁻¹ tunicamycin for another 6 h in 0.1% O₂) were subjected to co-immunoprecipitation with anti-HIF1 α antibody or rabbit IgG. IB, immunoblot. **c**, Schematic of the luciferase reporter constructs. 3xHRE reporter was co-transfected with doxycycline (dox)-inducible constructs encoding control or two XBP1 shRNAs into MDA-MB-231 cells. Cells were treated in 0.1% O₂ for 24 h and luciferase activity assayed. Experiments were performed in triplicate and data are shown as mean \pm s.d. **d**, Gene expression microarray heat map showing that genes involved in the HIF1 α -mediated hypoxia response were differentially expressed after XBP1 knockdown.

e, RT-PCR analysis of HIF1 α target gene expression after knockdown of XBP1 in MDA-MB-231-derived xenograft tumours in NOD/SCID/*Il2r γ −/−* mice. Results are presented relative to β -actin expression. *n* = 5. **f**, Plot showing the genome-wide association between the strength of XBP1 binding and the occurrence of the HIF1 α motif. The signal of XBP1 ChIP-seq peaks is shown as a heat map using red (the strongest signal) and white (the weakest signal) colour scheme. Each row shows \pm 300 bp centred on the XBP1 ChIP-seq peak summits. Rows are ranked by XBP1 occupancy. The horizontal blue lines denote the presence of the HIF1 α motif. **g, h**, Chromatin extracts from control, XBP1 knockdown (**g**) or HIF1 α knockdown (**h**) MDA-MB-231 cells (treated with 0.1% O₂ for 24 h) were subjected to ChIP using anti-HIF1 α (**g**) or anti-XBP1 antibodies (**h**). Data are shown as mean \pm s.d. of technical triplicates. Results show a representative of two independent experiments. **i**, Growth curve of tumours formed by MDA-MB-231 cells infected with inducible control shRNA (shCtrl), XBP1 shRNA (shXBP1) or XBP1 shRNA plus constitutively activated HIF1 α (shXBP1 + HIF1 α dPA). Mice were fed with doxycycline chow from day 7. Data are shown as mean \pm s.d. of biological replicates (*n* = 5). **P* < 0.05, ***P* < 0.01.

Co-immunoprecipitation experiments revealed a physical interaction of HIF1 α , but not HIF2 α , with XBP1 in 293T cells co-expressing HIF1 and XBP1s cultured under hypoxic conditions; an interaction was also observed with endogenous proteins in two TNBC cell lines: MDA-MB-231 and Hs578T (Fig. 3b and Extended Data Fig. 4h–j). Subcellular fractionation revealed that this interaction occurs in the nucleus, and that unspliced XBP1u protein was not detectable (Extended Data Fig. 4k, l). Glutathione S-transferase (GST) pull-down experiments showed that HIF1 α interacts with the XBP1s amino-terminus b-zip domain (Extended Data Fig. 4m, n).

We next established that XBP1 and HIF1 α co-occupied several well-known HIF1 α targets using ChIP-qPCR (Extended Data Fig. 5a–c). ChIP-re-ChIP assays using anti-XBP1s followed by anti-HIF1 α antibodies

confirmed that XBP1s and HIF1 α simultaneously co-occupy these common targets (Extended Data Fig. 5d). DNA pull-down assays with a HIF1 α (ref. 18) specific probe precipitated XBP1s in MDA-MB-231 nuclear extracts under hypoxia, indicating their presence in the same complex (Extended Data Fig. 5e, f). XBP1 depletion by two independent shRNA constructs markedly reduced hypoxia response element (HRE) luciferase activity under hypoxia (Fig. 3c). Conversely, XBP1s expression dose-dependently transactivated the HRE reporter (Extended Data Fig. 5g, h), confirming that XBP1 augments HIF1 α activity.

When we profiled the differential transcriptome induced by XBP1 silencing in MDA-MB-231 cells, gene-set enrichment analysis identified significant enrichment of HIF1 α -mediated hypoxia response pathway genes (Fig. 3d and Extended Data Fig. 6a). XBP1 depletion downregulated

HIF1 α targets VEGFA, PDK1, GLUT1 (also called SLC2A1) and DDIT4 expression in both normoxic and hypoxic conditions (Extended Data Fig. 6b), and these results were validated in breast cancer xenografts (Fig. 3e) and Hs578T cells (Extended Data Fig. 6c). However, XBP1 depletion in luminal tumours did not affect these targets (Extended Data Fig. 6d).

To explore the consequences of this cooperation further, we examined how XBP1 or HIF1 α loss affected the transcription of common target genes. We found that high XBP1 occupancy at its binding sites was associated with increased occurrence of the HIF1 α motif across the genome in TNBC (Fig. 3f). Whereas XBP1 depletion had no immediate effect on HIF1 α expression, it substantially attenuated concurrent HIF1 α and RNA polymerase II occupancy (Extended Data Fig. 6e–g).

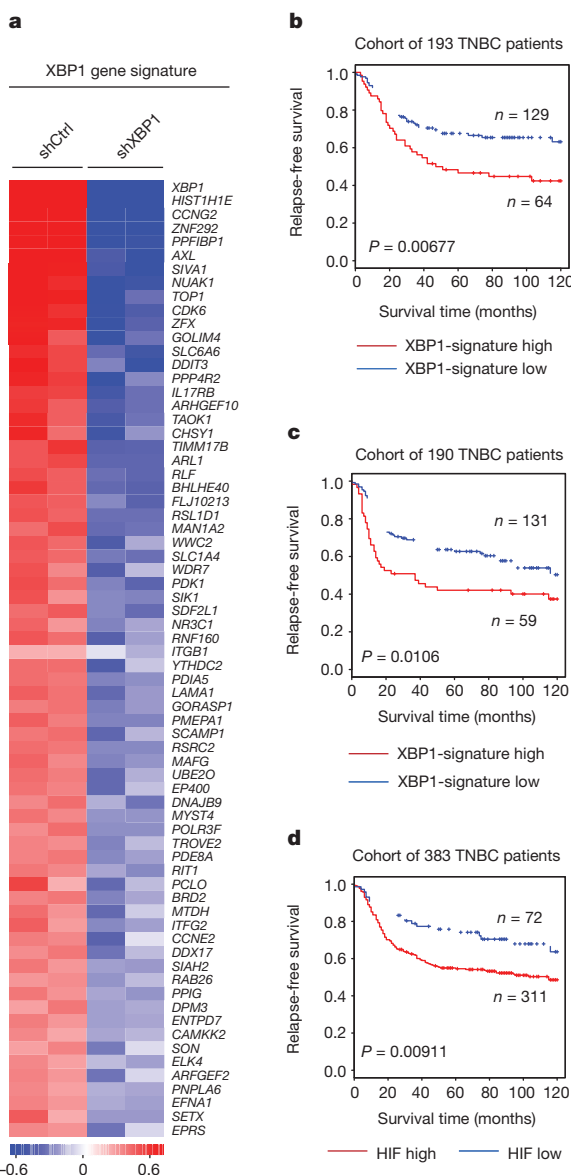


Figure 4 | XBP1 genetic signature is associated with human TNBC prognosis. **a**, Heat map showing the expression profile of genes bound by XBP1 and differentially expressed after *XBP1* knockdown. **b, c**, Kaplan–Meier graphs demonstrating a significant association between elevated expression of the XBP1 signature (red line) and shorter relapse-free survival in two cohorts of patients with TNBC (**b** and **c**). **d**, Kaplan–Meier graphs showing significant association of elevated HIF1 α gene signature expression (red line) with shorter relapse-free survival in a cohort of 383 TNBC patients. The log-rank test *P* values are shown.

and Fig. 3g). Similarly, XBP1 and RNA polymerase II occupancy at co-bound sites was likewise reduced in the absence of HIF1 α under hypoxic conditions (Fig. 3h and Extended Data Fig. 6h–l). These results indicate that the assembly of the XBP1–HIF1 α complex on target promoters is crucial for their transcription, via the recruitment of RNA polymerase II.

To establish whether HIF1 α contributes to the function of XBP1 in TNBC, we performed rescue experiments using a haemagglutinin (HA)-tagged constitutively activated hydroxylation-mutant HIF1 α construct (HA–HIF1 α dPA: P402A/P564A). XBP1 splicing was not directly regulated by HIF1 α (Extended Data Fig. 7a–c). Enforced overexpression of HIF1 α dPA in XBP1-depleted cells restored expression of HIF1 α targets and rescued anchorage-independent growth, mammosphere-forming ability, angiogenesis and *in vivo* tumour growth (Fig. 3i and Extended Data Fig. 7d–h). Conversely, HIF1 α silencing in XBP1s overexpressing cells markedly compromised their ability to sustain mammosphere formation (Extended Data Fig. 7i). Hypoxia is a physiological UPR inducer in cancer¹⁹ and XBP1s co-localizes with hypoxia marker CA9 in tumours²⁰. Our experiments demonstrate that XBP1 functions to sustain the hypoxia response via regulating the HIF1 α transcriptional program (Extended Data Fig. 8), which ensures maximum HIF activity and adaptive responses to the cytotoxic microenvironment of solid tumours.

Integrated analysis of XBP1 ChIP-seq data and gene expression profiles identified 96 genes directly bound and upregulated by XBP1. This gene set was defined as the XBP1 signature (Fig. 4a and Supplementary Table 1). Its expression was highly correlated with hypoxia-driven signatures in TNBC (Pearson's correlation coefficient = 0.61; *P* = 2.28×10^{-60}), but not in ER $^+$ breast cancer patients (coefficient = 0.03; *P* = 0.64) (Extended Data Fig. 9a, b). Survival analysis using an aggregate breast cancer data set for 193 TNBC patient samples²¹ demonstrated that tumours with an elevated XBP1 signature displayed shorter relapse-free survival (log-rank test, *P* = 0.00677) (Fig. 4b). Cox regression analysis showed that association of the signature with relapse-free survival remained significant after controlling for tumour size, grade and chemotherapy treatment (*P* = 0.00453, Supplementary Table 2). These findings were validated in a separate cohort of 190 TNBC patients (Fig. 4c). Importantly, the XBP1 signature did not correlate with clinical outcome of ER $^+$ breast cancer patients (*P* = 0.553) (Extended Data Fig. 9c), indicating its specific prognostic value for TNBC. Expression of the XBP1-regulated HIF1 α program was also associated with decreased relapse-free survival only in TNBC (*P* = 0.00911) (Fig. 4d and Extended Data Fig. 9d). Although XBP1 silencing also affects luminal breast cancer growth, it does so via a mechanism not involving HIF1 α (Extended Data Figs 4g, 6d and 10).

In conclusion, we have uncovered a key function of XBP1 in the tumorigenicity, progression and recurrence of TNBC, and have identified XBP1's control of the HIF1 α transcriptional program as the major mechanism. XBP1 pathway activation correlates with poor patient survival in TNBC patients, indicating that UPR inhibitors in combination with standard chemotherapy may improve the effectiveness of anti-tumour therapies.

METHODS SUMMARY

Orthotopic tumour growth assays. Female NOD/SCID/*Il2r γ* $^{−/−}$ or nude mice (Taconic) were injected orthotopically with 1.5×10^6 viable tumour cells re-suspended in 40 μ l Matrigel (BD Biosciences) into mammary glands and fed chow containing 6 g doxycycline per kg (Bioserv). For bioluminescent detection, mice were given a single intraperitoneal injection of luciferin, ketamine and xylazine and imaged with an IVIS imaging camera (Xenogen). Imaging intensity was normalized to the luminescence signal of individual mice before doxycycline chow treatment. The average luminescence ratio of treatment groups (*lacZ* or *XBP1* shRNA) was plotted over the course of doxycycline chow treatment and results presented as mean \pm s.d.

Mammosphere formation assay. Mammospheres were generated from cells in suspension (1,000 cells ml $^{−1}$) in serum-free DMEM/F12 media, supplemented with B27 (1:50, Invitrogen), 0.4% BSA, 20 ng ml $^{−1}$ EGF and 4 μ g ml $^{−1}$ insulin. After 6 days mammospheres were typically >75 μ m in size with $\sim 97\%$ CD44 high CD24 low . For serial passaging, 6-day-old mammospheres were collected, dissociated to single cells with trypsin and re-grown in suspension for 6 days.

Online Content Any additional Methods, Extended Data display items and Source Data are available in the online version of the paper; references unique to these sections appear only in the online paper.

Received 21 November 2012; accepted 31 January 2014.

Published online 23 March 2014.

1. Hanahan, D. & Weinberg, R. A. Hallmarks of cancer: the next generation. *Cell* **144**, 646–674 (2011).
2. Walter, P. & Ron, D. The unfolded protein response: from stress pathway to homeostatic regulation. *Science* **334**, 1081–1086 (2011).
3. Yoshida, H., Matsui, T., Yamamoto, A., Okada, T. & Mori, K. XBP1 mRNA is induced by ATF6 and spliced by IRE1 in response to ER stress to produce a highly active transcription factor. *Cell* **107**, 881–891 (2001).
4. Carrasco, D. R. et al. The differentiation and stress response factor XBP-1 drives multiple myeloma pathogenesis. *Cancer Cell* **11**, 349–360 (2007).
5. De Raedt, T. et al. Exploiting cancer cell vulnerabilities to develop a combination therapy for ras-driven tumors. *Cancer Cell* **20**, 400–413 (2011).
6. Mahoney, D. J. et al. Virus-tumor interactome screen reveals ER stress response can reprogram resistant cancers for oncolytic virus-triggered caspase-2 cell death. *Cancer Cell* **20**, 443–456 (2011).
7. Carey, L., Winer, E., Viale, G., Cameron, D. & Gianni, L. Triple-negative breast cancer: disease entity or title of convenience? *Nature Rev. Clin. Oncol.* **7**, 683–692 (2010).
8. Foulkes, W. D., Smith, I. E. & Reis-Filho, J. S. Triple-negative breast cancer. *N. Engl. J. Med.* **363**, 1938–1948 (2010).
9. Montagner, M. et al. SHARP1 suppresses breast cancer metastasis by promoting degradation of hypoxia-inducible factors. *Nature* **487**, 380–384 (2012).
10. The Cancer Genome Atlas Network. Comprehensive molecular portraits of human breast tumours. *Nature* **490**, 61–70 (2012).
11. Idowu, M. O. et al. CD44⁺/CD24^{-low} cancer stem/progenitor cells are more abundant in triple-negative invasive breast carcinoma phenotype and are associated with poor outcome. *Hum. Pathol.* **43**, 364–373 (2012).
12. Lin, Y., Zhong, Y., Guan, H., Zhang, X. & Sun, Q. CD44⁺/CD24⁻ phenotype contributes to malignant relapse following surgical resection and chemotherapy in patients with invasive ductal carcinoma. *J. Exp. Clin. Cancer Res.* **31**, 59 (2012).
13. Creighton, C. J. et al. Residual breast cancers after conventional therapy display mesenchymal as well as tumor-initiating features. *Proc. Natl Acad. Sci. USA* **106**, 13820–13825 (2009).
14. Iliopoulos, D., Hirsch, H. A. & Struhl, K. An epigenetic switch involving NF-κB, Lin28, Let-7 MicroRNA, and IL6 links inflammation to cell transformation. *Cell* **139**, 693–706 (2009).
15. Iliopoulos, D., Hirsch, H. A., Wang, G. & Struhl, K. Inducible formation of breast cancer stem cells and their dynamic equilibrium with non-stem cancer cells via IL6 secretion. *Proc. Natl Acad. Sci. USA* **108**, 1397–1402 (2011).
16. Schwab, L. P. et al. Hypoxia inducible factor-1α promotes primary tumor growth and tumor-initiating cell activity in breast cancer. *Breast Cancer Res.* **14**, R6 (2012).
17. Conley, S. J. et al. Antiangiogenic agents increase breast cancer stem cells via the generation of tumor hypoxia. *Proc. Natl Acad. Sci. USA* **109**, 2784–2789 (2012).
18. Yang, M. H. et al. Direct regulation of TWIST by HIF-1α promotes metastasis. *Nature Cell Biol.* **10**, 295–305 (2008).
19. Wouters, B. G. & Koritzinsky, M. Hypoxia signalling through mTOR and the unfolded protein response in cancer. *Nature Rev. Cancer* **8**, 851–864 (2008).
20. Spiotto, M. T. et al. Imaging the unfolded protein response in primary tumors reveals microenvironments with metabolic variations that predict tumor growth. *Cancer Res.* **70**, 78–88 (2011).
21. Rody, A. et al. A clinically relevant gene signature in triple negative and basal-like breast cancer. *Breast Cancer Res.* **13**, R97 (2011).
22. Barnard, G. A. A New Test for 2 × 2 Tables. *Nature* **156**, 177 (1945).
23. Barnard, G. A. Significance Tests for 2 × 2 Tables. *Biometrika* **34**, 123–138 (1947).

Supplementary Information is available in the online version of the paper.

Acknowledgements We thank W. G. Kaelin, A.-H. Lee, F. Martinon, M. N. Wein and X. Li for critical review of the manuscript. We are grateful to A. L. Richardson, H. Xu and J. Wang for advice and discussions. We thank L. A. Paskett, X. Liu, R. Kim and Y. Liu for technical support. This work was supported by the National Institutes of Health (CA112663 and AI32412 to L.H.G.; R01HG004069 to X.S.L.; K99CA175290 to Y.C.), the Leukemia and Lymphoma Society (to X.C.) and the National Natural Science Foundation of China (NSFC31329003 to X.S.L.).

Author Contributions X.C. and L.H.G. designed the research; X.C., D.I., Q.Z., M.B.G., M.H., E.L., D.Z.H., S.A., B.H., C.T. and M.S. did the experiments; Q.T. and Y.C. performed the bioinformatics analysis; X.S.L. supervised the bioinformatics analysis; M.N., W.L.T., M.B. and S.J.S. contributed to discussions and critical reagents; J.C.C., M.F., M.D.L., H.S. and J.M. contributed to the patient-derived xenograft experiments; X.C. and L.H.G. wrote the paper.

Author Information ChIP-seq and gene expression microarray data have been deposited in the NCBI Gene Expression Omnibus and are accessible through GEO series accession number GSE49955. Reprints and permissions information is available at www.nature.com/reprints. The authors declare competing financial interests: details are available in the online version of the paper. Readers are welcome to comment on the online version of the paper. Correspondence and requests for materials should be addressed to L.H.G. (lglimche@med.cornell.edu).

METHODS

Cell culture and treatments. The non-transformed breast cell line MCF10A contains an integrated fusion of the v-Src oncogene with the ligand-binding domain of the oestrogen receptor (ER-Src). These cells were grown in DMEM/F12 medium supplemented with 5% donor horse serum (Invitrogen), 20 ng ml⁻¹ epidermal growth factor (EGF) (R&D systems), 10 µg ml⁻¹ insulin (Sigma), 100 µg ml⁻¹ hydrocortisone (Sigma), 100 ng ml⁻¹ cholera toxin (Sigma), 50 units ml⁻¹ penicillin/streptomycin (Gibco), with the addition of puromycin (Sigma). Src induction and cellular transformation was achieved by treatment with 1 µM 4-OH tamoxifen, typically for 36 h, as described previously¹⁴.

All breast cancer cells were from ATCC cultured according to ref. 24. After retroviral or lentiviral infection, cells were maintained in the presence of puromycin (2 µg ml⁻¹) (Sigma). For all hypoxia experiments, cells were maintained in an anaerobic chamber (Coy laboratory) with 0.1% O₂. For glucose deprivation experiments, cells were maintained in DMEM without glucose medium (Gibco) with 10% FBS (Gibco) and 50 units ml⁻¹ of penicillin/streptomycin.

ChIP and ChIP-seq. ChIP was performed with XBP1 antibody (Biolegend, 619502); HIF1α antibody (Abcam, ab2185), RNA polymerase II antibody (Millipore, 05-623) or GST antibody (Santa Cruz, sc-33613) as described²⁵. See list of primers used in Fig. 3 (Supplementary Table 3). ChIP-seq libraries were prepared using the ChIP-Seq DNA Sample Prep kit (Illumina). XBP1 ChIP-seq peaks were first identified using MACS package with a *P* value cutoff of 1×10^{-7} on individual replicate. Correlations of the ChIP-seq signal in the union peak regions between two biological replicates are: MDA-MB-231_untreated, 0.97 ($P < 2.2 \times 10^{-16}$); MDA-MB-231_HG, 0.96 ($P < 2.2 \times 10^{-16}$); Hs578T_HG, 0.98 ($P < 2.2 \times 10^{-16}$); T47D_HG, 0.99 ($P < 2.2 \times 10^{-16}$). The correlations were calculated by cor.test() function in R (<http://www.r-project.org/>). The highly confident common peaks between replicates were further identified using an irreproducible discovery rate (IDR) cutoff of 20%. IDR is a statistical measure that assesses the consistency of the rank orders of the common ChIP-seq peaks between two replicates. The methodology and details of the implementation of IDR can be found in ref. 26.

Tumour initiation assay using patient-derived tumours. Tumour graft line BCM-2147 was derived by transplantation of a fresh patient breast tumour biopsy (ER⁺ PR⁺ HER2⁻) into the cleared mammary gland fat pad of immune-compromised SCID/Beige mice and retained the patient biomarker status and morphology across multiple transplant generations in mice. To overcome the challenge of limited cell viability by dissociation of solid tumours, 10 mg tumour pieces containing 1.3×10^5 cells were transplanted with basal membrane extract (Trevigen). The cell number was calculated as average cell yield 1.3×10^7 cells per gram $\times 0.01\text{ g} = 1.3 \times 10^5$ cells. For sustained siRNA release in the first 2 weeks after transplantation, porous silicon particles loaded with siRNA (scrambled control or *XBP1* siRNA) packaged in nanoliposomes were injected into the tumour tissue with basal membrane extract at the time of transplantation. Scrambled sequence, 5'-CGAACUGUGUGUGUGUG UGGCdTdT-3'; *XBP1* siRNA sequence 5'-CACCCUGAAUCAUUGUCUdTd T-3'. Two weeks after transplantation, nanoliposomes containing siRNA (15 mg per mouse) were injected intravenously twice weekly for 8 weeks. Mice were monitored thrice weekly for tumour development, and tumours were caliperized and recorded using LABCAT Tumour Analysis and Tracking System v6.4 (Innovative Programming Associates, Inc.). Tumour incidence is reported at 10 weeks after transplantation. The human patient samples were procured and used according to approved IRB protocols for research in human subjects.

Invasion assay. We performed invasion assays according to ref. 14. Invasion of the matrigel was conducted by using standardized conditions with BD BioCoat growth-factor-reduced matrigel invasion chambers (PharMingen). Assays were conducted according to manufacturer's protocol, by using 5% horse serum (Gibco) and 20 ng ml⁻¹ EGF (R&D Systems) as chemo-attractants.

Colony formation assay. 1×10^5 breast cancer cells were mixed 4:1 (v/v) with 2.0% agarose in growth medium for a final concentration of 0.4% agarose. The cell mixture was plated on top of a solidified layer of 0.8% agarose in growth medium. Cells were fed every 6–7 days with growth medium containing 0.4% agarose. The number of colonies was counted after 20 days. The experiment was repeated three times and the statistical significance was calculated using a Student's *t*-test.

Subcutaneous xenograft experiments. MCF10A ER-Src tamoxifen-treated (36 h) cells or MDA-MB-436 or HBL-100 breast cancer cells were injected subcutaneously in the right flank of athymic nude mice (Charles River Laboratories). Tumour growth was monitored every 5 days and tumour volumes were calculated by the equation $V(\text{mm}^3) = ab^2/2$, where *a* is the largest diameter and *b* is the perpendicular diameter. When the tumours reached a size of $\sim 100\text{ mm}^3$ (15 days) mice were randomly distributed into 3 groups (5 mice per group). The first group was used as control (non-treated), the second group was intratumorally treated with shCtrl and the third group was intratumorally treated with shXBP1. For each injection 10 µg of shRNA was mixed with 2 µl of vivo-jetPEI (polyethylenimine) reagent (catalogue no. 201-50G, PolyPlus Transfection SA) in a final volume of 100 µl. These treatments

were repeated every 5 days for 4 cycles (days 15, 20, 25 and 30). In addition, *in vivo* dilution xenotransplantation assays were performed in NOD/SCID/*Il2rγ*^{-/-} mice. Mice were evaluated on a weekly basis for tumour formation. All mice were maintained in accordance with Dana-Farber Cancer Institute Animal Care and Use Committee procedures and guidelines.

Purification of CD44^{high}CD24^{low} and CD44^{low}CD24^{high} cells from patients with TNBC. Five human invasive triple-negative ductal carcinoma tissues (stage III) were used in our experiments¹⁵. Immunomagnetic purification of CD44^{high}CD24^{low} and CD44^{low}CD24^{high} cells was performed according to ref. 27. Briefly, the breast tissues were minced into small pieces (1 mm) using a sterile razor blade. The tissues were digested with 2 mg ml⁻¹ collagenase I (C0130, Sigma) and 2 mg ml⁻¹ hyaluronidase (H3506, Sigma) in 37 °C for 3 h. Cells were filtered, washed with PBS and followed by Percoll gradient centrifugation. The first purification step was to remove the immune cells by immunomagnetic purification using an equal mix of CD45 (leukocytes), CD15 (granulocytes), CD14 (monocytes) and CD19 (B cells) Dynabeads (Invitrogen). The second purification step was to isolate fibroblasts from the cell population by using CD10 beads for magnetic purification. The third step was to isolate the endothelial cells by using an 'endothelial cocktail' of beads (CD31 BD Pharmingen catalogue no. 555444, CD146 P1H12 MCAM BD Pharmingen catalogue no. 550314, CD105 Abcam catalogue no. Ab2529, cadherin 5 Immunotech catalogue no. 1597, and CD34 BD Pharmingen catalogue no. 555820). In the final step the CD44^{high} cells were purified from the remaining cell population using CD44 beads. These cells were sorted for CD44^{high}CD24^{low} cells, CD24^{high} cells were also purified using CD24 beads. These cells were sorted for CD44^{low}CD24^{high} cells. These cell populations were sorted again with CD44 antibody (FITC-conjugated) (555478, BD Biosciences) and CD24 antibody (PE-conjugated) (555428, BD Biosciences) to increase their purity (>99.2% in all cases).

Gene expression microarray analysis. MDA-MB-231 cells infected with control shRNA or *XBP1* shRNA lentiviruses grown in glucose-free medium were treated in 0.1% O₂ in a hypoxia chamber for 24 h. Total RNA was extracted by using RNeasy mini kit with on column DNase digestion (Qiagen). Biotin-labelled cRNA was prepared from 1 µg of total RNA, fragmented, and hybridized to Affymetrix human U133 plus 2.0 expression array. All gene expression microarray data were normalized and summarized using RMA. The differentially expressed genes were identified using Limma ($q \leq 10\%$).

Motif analysis. Flanking sequences around the summits (± 300 bp) of the top 1,000 *XBP1* binding sites were extracted and the repetitive regions in these flanking sequences were masked. The consensus sequence motifs were derived using Seqpos.

XBP1 signature generation. The *XBP1* signature was generated by integrative analysis of ChIP-seq and differential expression data using the method as previously described²⁸. Briefly, we first calculated the regulatory potential for a given gene, *S_g*, as the sum of the nearby binding sites weighted by the distance from each site to the transcription start site (TSS) of the gene $S_g = \sum_{i=1}^k e^{-(0.5+4\Delta_i)}$, where *k* is the number of binding sites within 100 kb of gene *g* and Δ_i is the distance between site *i* and the TSS of gene *g* normalized to 100 kb (for example, 0.5 for a 50-kb distance). We then applied the Breitling's rank product method to combine regulatory potentials with differential expression *t*-values to rank all genes based on the probability that they were *XBP1* targets. Only genes with at least one binding site within 100 kb from its TSS and a differential expression *t*-value above the 75th percentile were considered. The FDR of *XBP1* target prediction was estimated by permutation. At a FDR cutoff of 20% and differential expression fold-change cutoff of 1.5, we obtained 96 upregulated genes (HUGO gene symbol) as direct targets of *XBP1*.

Survival analysis. We performed survival analysis using an aggregated compendium of gene expression profiles of 383 TNBC samples from 21 breast cancer data sets²¹. Of the 96 *XBP1* signature genes, 70 genes had corresponding probes in this data set. To avoid potential confounding factors such as heterogeneity among the samples, we randomly split all 383 TNBC samples into two data sets with similar size (193 and 190 cases) and evaluated the correlation of the *XBP1* gene signature with relapse-free survival using these two data sets, respectively. We separated patients into two subgroups: one with higher and the other with lower expression of the *XBP1* signature. The subgroup classification was performed as described previously²⁹. Patients were considered to have a higher *XBP1* signature if they had average expression values of all the genes in the *XBP1* signature above the 58th percentile²⁹. Kaplan–Meier survival analysis was performed and log-rank test was used to assess the statistical significance of survival difference between these two groups. We also performed multivariate Cox regression analysis to evaluate the significance of the association between *XBP1* signature and relapse-free survival in the presence of other clinical variables including tumour stage, tumour grade and the treatment with chemotherapy. A similar analysis was performed for the HIF pathway signature (VEGFA, PDK1, DDIT4, SLC2A1, KDM3A, NDRG1, PFKFB3,

PIK3CA, RORB, CREBBP, PIK3CB, HK2 and EGLN1). Similar to the analysis for TNBC, the survival analysis was performed for ER⁺ breast cancer using gene expression profiles and clinical annotations of 209 ER⁺ breast cancer patients³⁰.

Virus production and infection. The Phoenix packaging cell line was used for the generation of ecotropic retroviruses and the 293T packaging cell line was used for lentiviral amplification. In brief, viruses were collected 48 and 72 h after transfection, filtered, and used for infecting cells in the presence of 8 µg ml⁻¹ polybrene before drug selection with puromycin (2 µg ml⁻¹). shRNA constructs were generated by The Broad Institute. Targeting of GFP mRNA with shRNA served as a control. Optimal targeting sequences identified for human *XBP1* were 5'-GACCC AGTCATTTCTTCAAA-3', and 5'-GAACAGCAAGTGGTAGATTAA-3', respectively. Knockdown efficiency was assessed by real-time PCR for *XBP1*.

Luciferase assay. For Extended Data Fig. 5g, MDA-MB-231 cells were co-transfected with 3×HRE luciferase (3×HRE-Luc) plasmid and *XBP1*s overexpression construct or control vector by using Lipofectamine 2000 (Invitrogen). A Renilla luciferase plasmid (pRL-CMV from Promega) was co-transfected as an internal control. Cells were collected 36 h after transfection, and the luciferase activities of the cell lysates were measured by using the Dual-luciferase Reporter Assay System (Promega). For Fig. 3c, MDA-MB-231 cells were co-transfected with 3×HRE-Luc and two inducible *XBP1* shRNA constructs (in pLKO-Tet-On vector) or control shRNA construct by using Lipofectamine 2000 (Invitrogen). Cells were treated with doxycycline for 48 h and hypoxia for 24 h before the luciferase activities of the cell lysates were measured.

Statistical analysis. The significance of differences between treatment groups was measured with a Student's *t*-test. *P* values of less than 0.05 were considered statistically significant.

Co-immunoprecipitation. Transfected cells were lysed in cell lysis buffer (50 mM Tris HCl, pH 8.0, 150 mM NaCl, 1 mM EDTA, 1% Nonidet P-40, and 10% glycerol with protease inhibitor cocktail) for 1 h. M2 beads (Sigma) were incubated with the whole-cell extracts at 4 °C overnight. The beads were washed with cell lysis buffer four times. Finally, the beads were boiled in 2× sample buffer for 10 min. The eluents were analysed by western blot. Nuclear extracts were used to perform the endogenous co-immunoprecipitation. Briefly, 5 mg of nuclear extracts were incubated with 5 µg of anti-HIF1α antibody (Novus Biologicals, NB100-479) at 4 °C overnight. The protein complexes were precipitated by addition of protein A agarose beads (Roche) with incubation for 4 h at 4 °C. The beads were washed four times and boiled for 5 min in 2× sample buffer.

Real-time PCR analysis. 1 µg of RNA sample was reverse-transcribed to form cDNA, which was subjected to SYBR-green-based real-time PCR analysis. Primers used for β-actin forward: 5'-CCTGTACGCCAACACAGTC-3' and reverse 5'-ATACTCCTGCTTGATCC-3'; for VEGFA forward 5'-CACACAGGATG GCTTGAAGA-3' and reverse 5'-AGGGCAGAACATCACGAAG-3'; for PDK1 forward 5'-GGAGGTCTAACACAGGAGTC-3' and reverse 5'-GTTCATGTCA CGCTGGTAA-3'; for GLUT1 forward 5'-TGGACCCATGTCTGGTTGTA-3' and reverse 5'-ATGGAGCCCAGCAGCAA-3'; for JMJD1A forward 5'-TCAGG TGACTTTGTTTCAGC-3' and reverse 5'-CACCGACGTTACCAAGAAGG-3'; for DDT4 forward 5'-CATCAGGTTGGCACACAAGT-3' and reverse 5'-CCT GGAGAGCTCGGACTG-3'; for MCT4 forward 5'-TACATGTAGACGTGGG TCGC-3' and reverse 5'-CTGCAGTTGAGGTGCTCAT-3'; for *XBP1* splicing forward 5'-CCTGGTTGCTGAAGAGGAGG-3' and reverse 5'-CCATGGGGAG ATGTTCTGGAG-3'; for *XBP1* total forward 5'-AGGAGTTAACAGACAGCGCT TGGGGATGGGAT-3' and reverse 5'-CTGAATCTGAAGAGTCATAACGCCA GAAT-3'.

ChIP-re-ChIP. *XBP1* antibody was crosslinked to protein G-Sepharose beads using dimethylpimelimidate to prevent the leaching of antibody during sodium dodecyl sulphate (SDS) elution. The beads were then incubated with chromatin extracts overnight. Subsequently, the beads were washed and eluted with 1% SDS elution buffer at 37 °C for 45 min. The eluate was diluted to a final SDS concentration of 0.1% and incubated with fresh antibody-bound beads for the second immunoprecipitation. For the final round of immunoprecipitation, washed beads were eluted with 1% SDS elution buffer at 68 °C for 30 min. Eluate was de-crosslinked in the

presence of pronase and heated at 68 °C for 6 h, and DNA was purified by phenol-chloroform extraction.

Glutathione S-transferase pull-down assay. Various deletion fragments of *XBP1*s were cloned into pET42b (Novagen). The plasmids were transformed into BL21 *Escherichia coli*. The *XBP1*s proteins were expressed and purified with glutathione (GSH)-Sepharose beads (GE Healthcare). The purified proteins were bound to GSH beads and incubated with HIF1α-overexpressed cell lysates for 2 h in 4 °C. The beads were washed six times with cell lysis buffer. The eluents were analysed by western blot.

DNA-binding assay. Nuclear protein (150 µg) was incubated for 1 h at 4 °C with a biotinylated probe containing wild-type or mutated HIF1α binding site plus streptavidin-dynabeads (Invitrogen) in binding buffer (100 mM NaCl, 10 mM Tris-HCl, pH 7.6, 0.1 mM EDTA, 1 mM dithiothreitol, 5% glycerol, 1 mg ml⁻¹ of BSA and 20 µg ml⁻¹ of poly(dI:dC), plus protease inhibitors). Streptavidin beads were washed in binding buffer, and bound proteins were analysed by immunoblot for *XBP1*s or HIF1α.

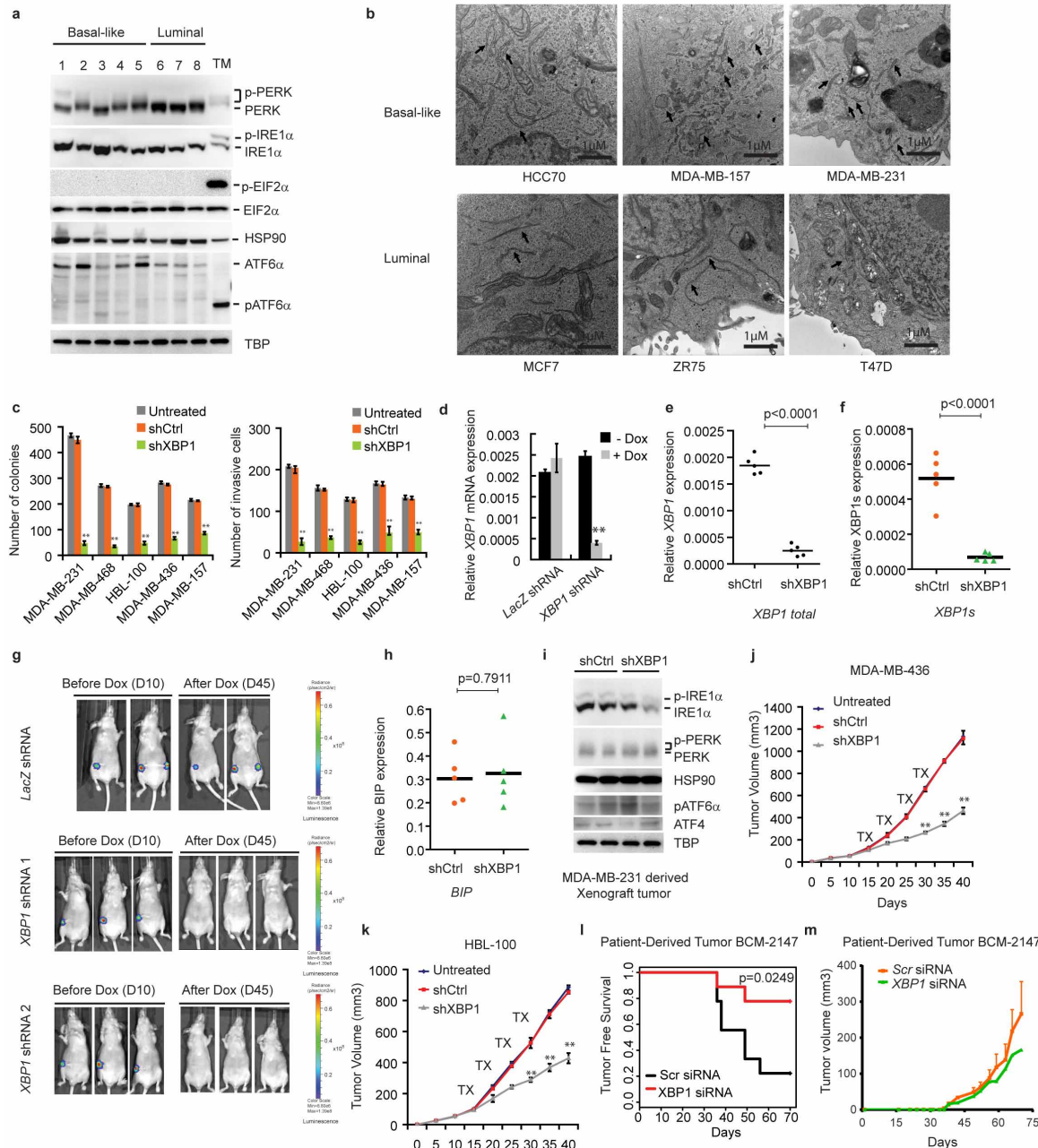
Transmission electron microscopy. Cells were washed with serum-free media then fixed with a modified Karmovsky's fix of 2.5% glutaraldehyde, 4% paraformaldehyde and 0.02% picric acid in 0.1 M sodium cacodylate buffer at pH 7.2. After a secondary fixation in 1% osmium tetroxide, 1.5% potassium ferricyanide, samples were dehydrated through a graded ethanol series, and embedded *in situ* in an epon analogue resin. En face ultrathin sections were cut on a Leica Ultracut S Ultramicrotome (Leica). Sections were collected on copper grids and further contrasted with lead citrate and viewed on a JEM 1400 electron microscope (JEOL) operated at 100 kV. Digital images were captured on a Veleta 2K × 2K CCD camera (Olympus-SIS).

Caspase 3 ELISA assay. Quantification of cleaved caspase-3 activity was performed using the PathScan Cleaved Caspase-3 (Asp175) sandwich ELISA kit (no. 7190, Cell Signaling) according to the manufacturer's recommendations.

Immunohistochemical staining. We fixed xenograft tumour tissues in 4% paraformaldehyde and performed immunohistochemistry on 5-µm-thick paraffin sections after heat-induced antigen retrieval. The following primary antibodies were used: CD31 (1:50, Abcam, ab28364), cleaved caspase 3 (1:200, Cell Signaling, 9664), CD44 (1:100, Novocastra), Ki67 (1:50, Dako, Clone MIB-1), and carbonic anhydrase IX (1:40, Novus Biologicals). Subsequently, we incubated the slides with biotinylated secondary antibody and ABC-HRP (both from Vector Lab). EnVision+ system (Dako) was used to amplify caspase 3 and carbonic anhydrase IX. Mouse on Mouse ImmPRESS Polymer kit (Vector Lab) was applied to increase CD44 signal-to-noise ratio. For all slides, final detectable signal was visualized by DAB as the location of antigens. After counterstaining with haematoxylin, slides were mounted.

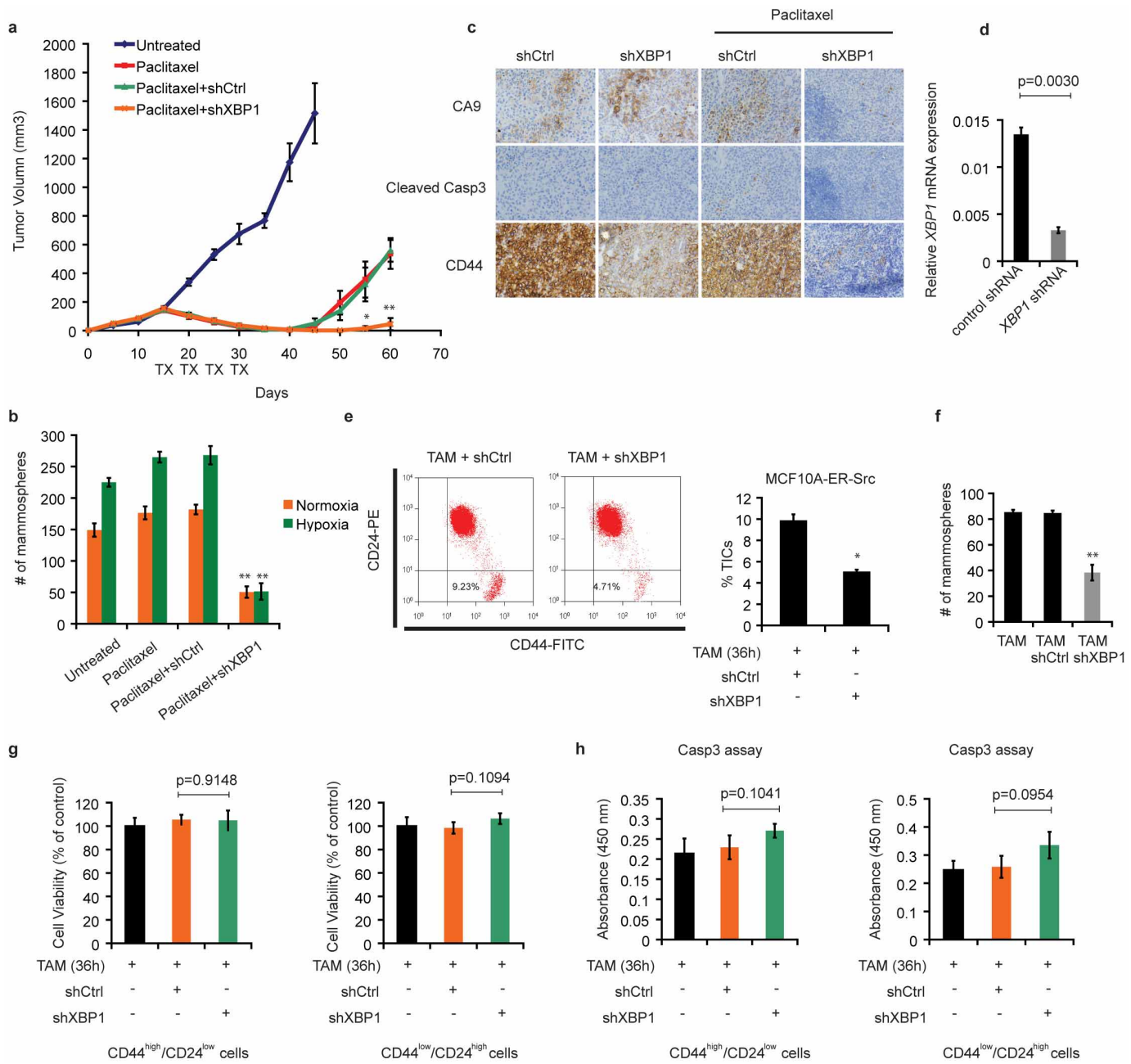
Immunoblot analysis. Total cell extracts or nuclear extracts were separated by SDS-PAGE and transferred to PVDF membranes. IRE1α phosphorylation was monitored by Phos-tag SDS-PAGE. PERK phosphorylation was monitored by 5% SDS-PAGE. The following antibodies were used for immunoblot analysis: anti-*XBP1*s (BioLegend, 619502); anti-PERK (Cell Signaling, 5683); anti-IRE1α (Cell Signaling, 3294); anti-ATF6 (Cosmo bio, BAM-73-500-EX); anti-ATF4 (Santa Cruz, sc-200); anti-Hsp90 (Santa Cruz, sc-7947); anti-TBP (Abcam, 51841); anti-EIF2α (Santa Cruz, sc-11386); anti-phospho-EIF2α (Cell Signaling, 9721).

24. Neve, R. M. *et al.* A collection of breast cancer cell lines for the study of functionally distinct cancer subtypes. *Cancer Cell* **10**, 515–527 (2006).
25. Chen, X. *et al.* Integration of external signaling pathways with the core transcriptional network in embryonic stem cells. *Cell* **133**, 1106–1117 (2008).
26. Li, Q., Brown, J. B., Huang, H. & Bickel, P. J. Measuring reproducibility of high-throughput experiments. *Ann. Appl. Stat.* **5**, 1752–1779 (2011).
27. Shipitsin, M. *et al.* Molecular definition of breast tumor heterogeneity. *Cancer Cell* **11**, 259–273 (2007).
28. Tang, Q. *et al.* A comprehensive view of nuclear receptor cancer cistromes. *Cancer Res.* **71**, 6940–6947 (2011).
29. Marotta, L. L. *et al.* The JAK2/STAT3 signaling pathway is required for growth of CD44⁺CD24⁻ stem cell-like breast cancer cells in human tumors. *J. Clin. Invest.* **121**, 2723–2735 (2011).
30. Wang, Y. *et al.* Gene-expression profiles to predict distant metastasis of lymph-node-negative primary breast cancer. *Lancet* **365**, 671–679 (2005).



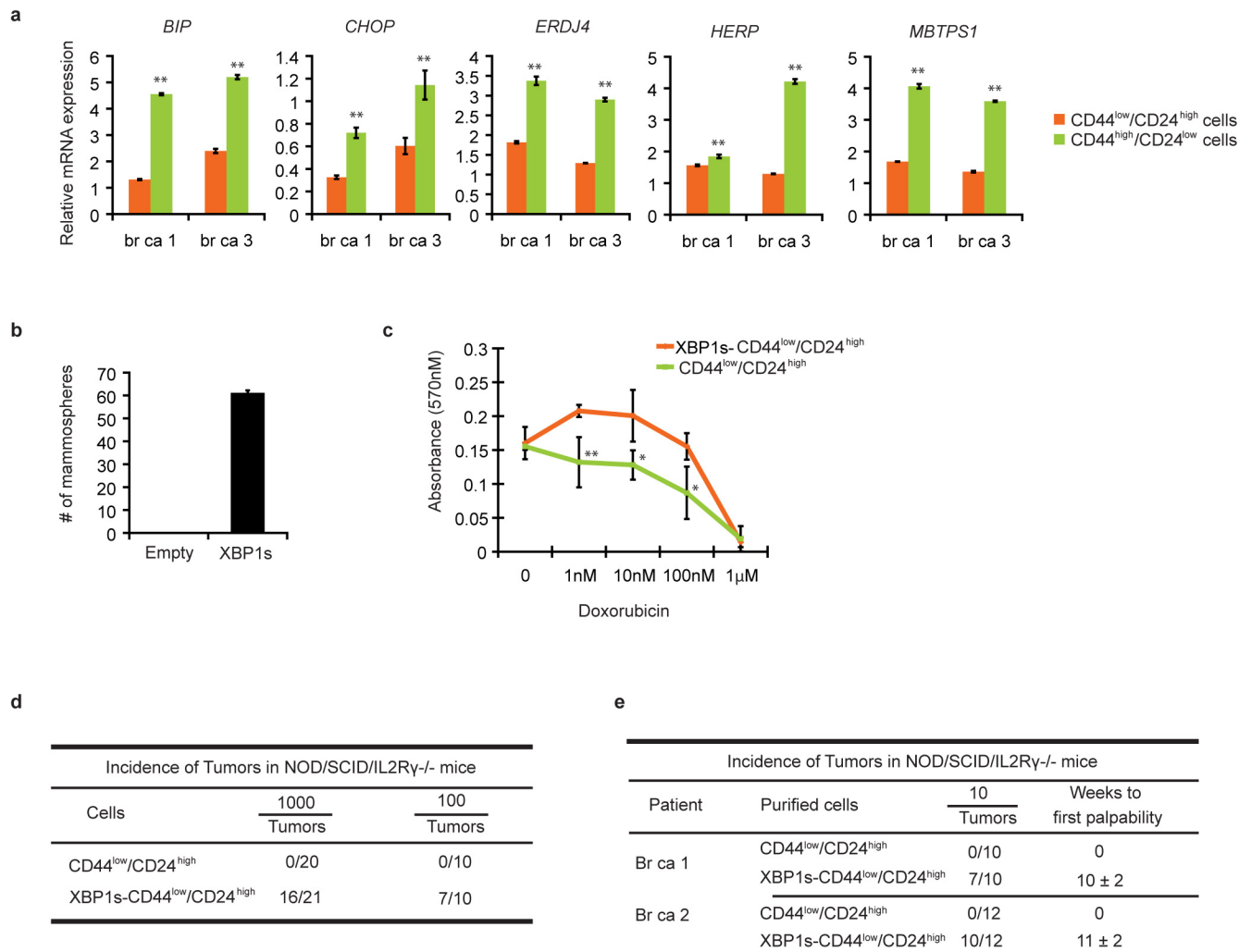
Extended Data Figure 1 | Effect of *XBP1* silencing on TNBC cells and UPR. **a**, Activation of UPR in different breast cancer cells. Immunoblot of PERK phosphorylation, IRE1 α activation (phos-tag SDS-PAGE) and EIF2 α phosphorylation in whole-cell lysates, and ATF6 α processing (pATF6 α) in nuclear extract of basal-like breast cancer cells (1, HCC1937; 2, MDA-MB-231; 3, SUM159; 4, MDA-MB-157; 5, HCC70) and luminal breast cancer cells (6, ZR-75-1; 7, T47D; 8, MCF7). TM, positive control (whole-cell lysates or nuclear extracts from MDA-MB-231 cells treated with 5 μ g ml $^{-1}$ tunicamycin for 6 h). HSP90 was used as loading control for whole-cell lysates, TBP was used as loading control for nuclear extract. **b**, Transmission electron microscopic analysis of ER in basal-like and luminal breast cancer cell lines. Black arrows indicate the endoplasmic reticulum. All images are at original magnification of 30,000 \times . Scale bar, 1 μ M. **c**, Quantification of soft agar colony formation and number of invasive cells in untreated and control shRNA or *XBP1* shRNA infected breast cancer cells. Experiments were performed in triplicate and data are shown as mean \pm s.d. $^{**}P < 0.01$. **d**, Quantitative RT-PCR analysis of *XBP1* expression in MDA-MB-231 cells infected with lentiviruses encoding doxycycline (dox) inducible shRNAs against *XBP1* or scrambled LacZ control, in the presence or absence of doxycycline for 48 h. Data are presented relative to β -actin and shown as mean \pm s.d. of technical triplicates. **e**, **f**, Knockdown efficiency of total *XBP1* (**e**) and *XBP1*s (**f**) in MDA-MB-231-derived xenograft

tumour (as in Fig. 1d). Data are presented relative to β -actin. $n = 5$. **g**, Bioluminescent images of orthotopic tumours formed by luciferase-expressing MDA-MB-231 cells infected with different lentiviruses. A total of 1.5×10^6 cells were injected into the fourth mammary glands of nude mice. Bioluminescent images were obtained 1 week later and serially after mice were begun on chow containing doxycycline (dox) (day 10). Pictures shown are the day 10 images (before dox) and day 45 images (after dox). **h**, Effect of *XBP1* knockdown on ER stress marker BIP expression in MDA-MB-231-derived xenograft tumours. Quantitative RT-PCR analysis of *BIP* expression in shCtrl or shXBP1 xenograft tumour. Data are presented relative to β -actin. $n = 5$. **i**, Immunoblot of IRE1 α activation (phos-tag SDS-PAGE) and PERK phosphorylation in whole-cell lysates; ATF6 α processing and ATF4 expression in nuclear extracts of two shCtrl or shXBP1 xenograft tumours. HSP90 was used as loading control for whole-cell lysates; TBP was used as loading control for nuclear extract. **j**, **k**, Tumour growth of untreated or control shRNA, or *XBP1* shRNA treated MDA-MB-436 (**j**) or HBL-100 cells (**k**) in nude mice. Data are shown as mean \pm s.d. of biological replicates ($n = 3$). $^{**}P < 0.01$. Tx: treatment with shRNA. **l**, Kaplan-Meier tumour-free survival curve of mice from Fig. 1f. **m**, Tumour growth (mean \pm s.e.m.) of BCM-2147 tumours as in Fig. 1f (Scr siRNA, $n = 7$; *XBP1* siRNA, $n = 2$).



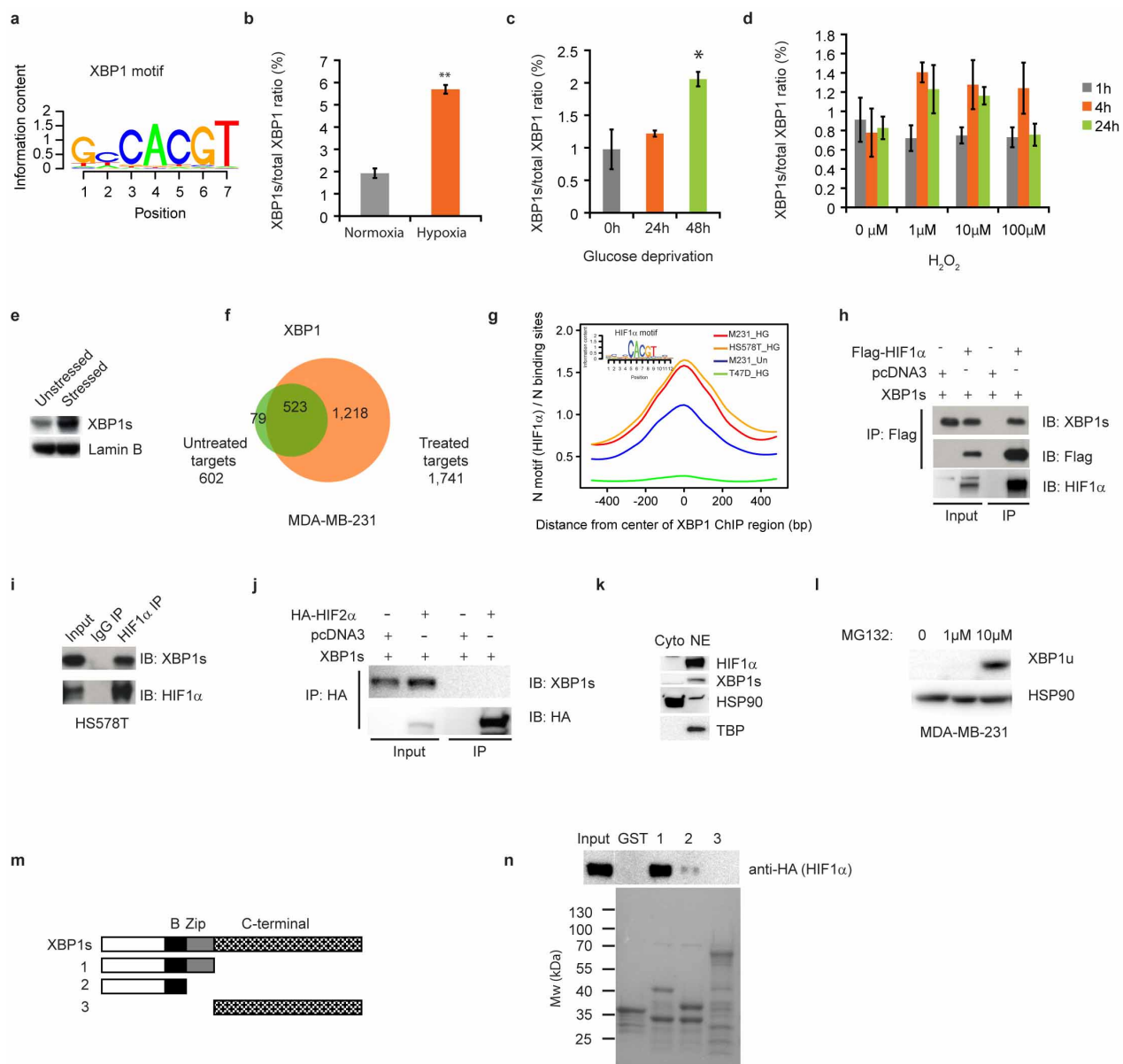
Extended Data Figure 2 | Effect of XBP1 on tumour relapse and CD44^{high}CD24^{low} cells. **a**, Tumour growth of MDA-MB-231 cells untreated or treated with paclitaxel (20 mg kg⁻¹), or paclitaxel + control shRNA, or paclitaxel + XBP1 shRNA in nude mice. TX, treatment with paclitaxel or paclitaxel + shRNA. Data are shown as mean ± s.d. of biological replicates ($n = 5$). **b**, Number of mammospheres per 1,000 cells generated from day 20 xenograft tumours under different treatments as indicated under normoxic or hypoxic condition (0.1% O₂). Data are shown as mean ± s.d. of biological replicates ($n = 3$). Asterisk denotes significantly different from paclitaxel + shCtrl control in each treatment; * $P < 0.05$, ** $P < 0.01$. **c**, Effect of XBP1 knockdown on cell death in hypoxic regions (assessed by CA9 and cleaved caspase 3 staining) or accumulation of CD44^{high}CD24^{low} cells (assessed by CD44 staining). Immunohistochemical staining of CA9 and cleaved caspase 3 (consecutive sections) showed that cell death was not induced in hypoxic region in XBP1 knockdown tumours. Immunohistochemical staining of CD44 showed significant reduction of CD44 expression in XBP1 knockdown tumours. All tumour sections are from MDA-MB-231-derived xenograft with different treatment as indicated. **d**, Knockdown efficiency of XBP1 in MCF10A-ER-Src cells. Data are shown as mean ± s.d. of technical triplicates.

e, Left panel: flow cytometry analysis of CD44 and CD24 expression of tamoxifen-treated (36 h) MCF10A ER-Src cells infected with control shRNA or XBP1 shRNA encoding lentivirus. Right panel: percentage of CD44^{high}CD24^{low} cells in tamoxifen (4-OH-tamoxifen)-treated MCF10A-ER-Src cells infected with control shRNA or XBP1 shRNA encoding lentivirus. Experiments were performed in triplicate and data are shown as mean ± s.d. * $P < 0.05$. **f**, Number of mammospheres per 1,000 cells generated by tamoxifen-treated MCF10A ER-Src cells uninfected, or infected with control shRNA or XBP1 shRNA encoding lentivirus. Experiments were performed in triplicate and data are shown as mean ± s.d. **g**, Cell viability assay (Cell-titer Glo) on CD44^{high}CD24^{low} or CD44^{low}CD24^{high} cells isolated from tamoxifen-treated MCF10A-ER-Src cells infected with control shRNA or XBP1 shRNA encoding lentivirus (72 h after infection). Data were normalized to the control (cell infected with shCtrl). Experiments were performed in triplicate and data are shown as mean ± s.d. **h**, Cleaved caspase 3 ELISA assays on CD44^{high}CD24^{low} or CD44^{low}CD24^{high} cells isolated from tamoxifen-treated MCF10A-ER-Src cells infected with control shRNA or XBP1 shRNA encoding lentivirus (72 h after infection). Experiments were performed in triplicate and data are shown as mean ± s.d.



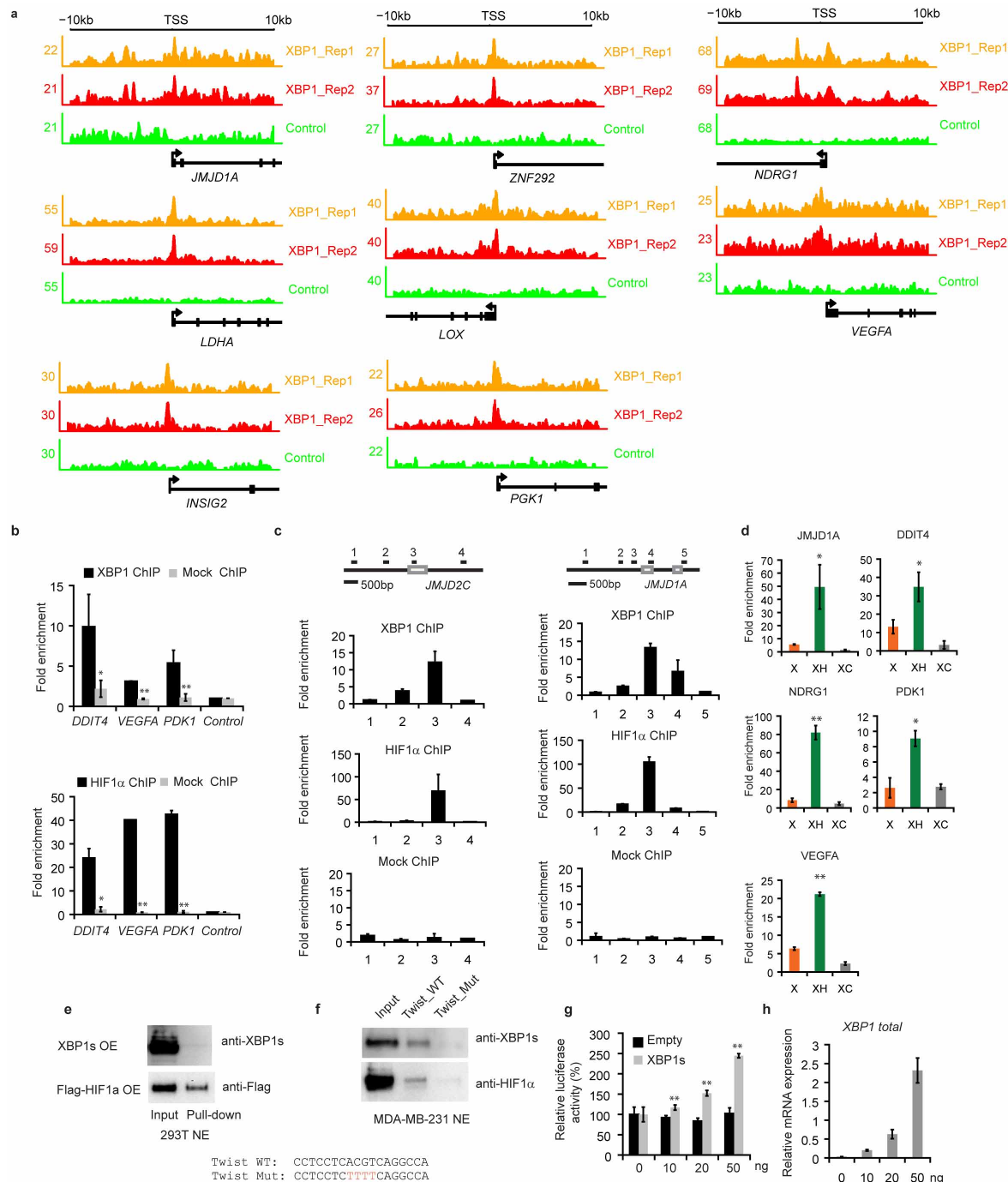
Extended Data Figure 3 | Effect of XBP1 on CD44^{high}CD24^{low} cells. **a**, UPR markers are upregulated in CD44^{high}CD24^{low} cells. Quantitative RT-PCR analysis of UPR markers *BIP*, *CHOP*, *ERDJ4*, *HERP* and *MBTPS1* in CD44^{low}CD24^{high} cells and CD44^{high}CD24^{low} cells sorted from two TNBC patients. Data are shown as mean ± s.d. of technical triplicates. **P* < 0.05, ***P* < 0.01. **b**, XBP1s overexpression in CD44^{low}CD24^{high} cells generates mammosphere-forming ability. Number of mammospheres per 1,000 cells generated by sorted CD44^{low}CD24^{high} cells transduced with empty vector or XBP1s expressing retrovirus. Experiments were performed in triplicate and data are shown as mean ± s.d. **c**, CD44^{low}CD24^{high} cells overexpressing XBP1s are more resistant to chemotherapy. MTT (3-[4,5-dimethylthiazol-2-yl]-2,5-

diphenyl tetrazolium bromide) assay was performed to measure the dose-response curves of CD44^{low}CD24^{high} cells or CD44^{low}CD24^{high} cells expressing XBP1s treated with doxorubicin. Experiments were performed in triplicate and data are shown as mean ± s.d. **P* < 0.05, ***P* < 0.01. **d**, 1,000 or 100 CD44^{low}CD24^{high} cells sorted from transformed MCF10A ER-Src cells or CD44^{low}CD24^{high} cells overexpressing XBP1s were injected into NOD/SCID/IL2R $\gamma^{-/-}$ mice and the incidence of tumours was monitored. **e**, Ten CD44^{low}CD24^{high} cells sorted from two human patients with TNBC or CD44^{low}CD24^{high} cells overexpressing XBP1s were injected into NOD/SCID/IL2R $\gamma^{-/-}$ mice and the incidence of tumours was monitored.



Extended Data Figure 4 | HIF1α is a co-regulator of XBP1. **a**, Identification of XBP1 motif in MDA-MB-231 ChIP-seq data set. Matrices predicted by the *de novo* motif-discovery algorithm Seqpos. $P < 1.08 \times 10^{-30}$. **b**, Induction of XBP1 splicing by hypoxia. RT-PCR analysis of the ratio of XBP1s to total XBP1 in MDA-MB-231 cells cultured under normoxic condition or hypoxic condition (0.1% O₂) for 24 h. Data are shown as mean \pm s.d. of technical triplicates. ** $P < 0.01$. **c**, Induction of XBP1 splicing by glucose deprivation. RT-PCR analysis of the ratio of XBP1s to total XBP1 in MDA-MB-231 cells cultured in normal medium or glucose-free medium for 24 h or 48 h. Data are shown as mean \pm s.d. of technical triplicates. * $P < 0.05$. **d**, Induction of XBP1 splicing by oxidative stress. RT-PCR analysis of the ratio of XBP1s to total XBP1 in MDA-MB-231 cells untreated or treated with different doses of H₂O₂ for 1 h, 4 h or 24 h. Data are shown as mean \pm s.d. of technical triplicates. **e**, Western blotting analysis of XBP1s expression in nuclear extract of MDA-MB-231 cells cultured under normoxia or hypoxia (0.1% O₂) and glucose-free condition for 16 h. Lamin B was used as loading control. **f**, Venn diagram showing the overlap between XBP1 targets in MDA-MB-231 breast cancer cells cultured under normoxic conditions (untreated) or hypoxia and glucose deprivation conditions (treated). **g**, Motif enrichment analysis in the XBP1 binding sites in untreated or stressed (0.1% O₂) and glucose deprivation (HG) MDA-MB-231, Hs578T or T47D cells. The 1-kb region surrounding the summit of the XBP1 peak is equally divided into 50 bins. The average HIF1α motif occurrence over top 1,000 XBP1 peaks in each bin is plotted. The corresponding P values of each condition are listed as follows: M231_Un, 7.78×10^{-20} ; M231_HG, $< 1.08 \times 10^{-30}$; Hs578T_HG, $< 1.08 \times 10^{-30}$; T47D_HG, 6.14×10^{-6} . **h**, Flag-tagged HIF1α and XBP1s were co-expressed in 293T cells, and the cells were treated in 0.1% O₂ for 16 h. Co-immunoprecipitation was performed with M2 anti-Flag antibody. Western blot was carried out with anti-XBP1s antibody, anti-Flag antibody or anti-HIF1α antibody. Empty vector was used as control. **i**, Nuclear extracts from Hs578T cells treated with tunicamycin (1 μ g ml⁻¹, 6 h) in 0.1% O₂ (16 h) were subjected to co-immunoprecipitation with anti-HIF1α antibody or rabbit IgG. Western blot was carried out with anti-XBP1s antibody or anti-HIF1α antibody. **j**, HA-tagged HIF2α and XBP1s were co-expressed in 293T cells, and the cells were treated in 0.1% O₂ for 16 h. Co-immunoprecipitation was performed with anti-HA antibody. Western blot was carried out with anti-XBP1s antibody or anti-HA antibody. Empty vector was used as control. **k**, Localization of XBP1s and HIF1α in MDA-MB-231 cells. Western blotting analysis of XBP1s and HIF1α expression in cytosolic extracts and nuclear extracts of MDA-MB-231 cells cultured under 0.1% O₂ condition for 24 h. HSP90 and TBP were used as control. **l**, XBP1u is not expressed in MDA-MB-231 cells. Western blotting analysis of XBP1u in MDA-MB-231 cells untreated or treated with 1 μ M or 10 μ M MG132 for 4 h. HSP90 was used as loading control. **m**, Schematic diagram of full-length and truncated forms of XBP1s protein. **n**, A GST pull-down assay was performed using GST-tagged XBP1s proteins and 293T cell lysates overexpressing HA-tagged HIF1α. Western blotting was performed with an anti-HA antibody. Lower panel: Coomassie blue staining of GST-tagged different truncated forms of XBP1s proteins.

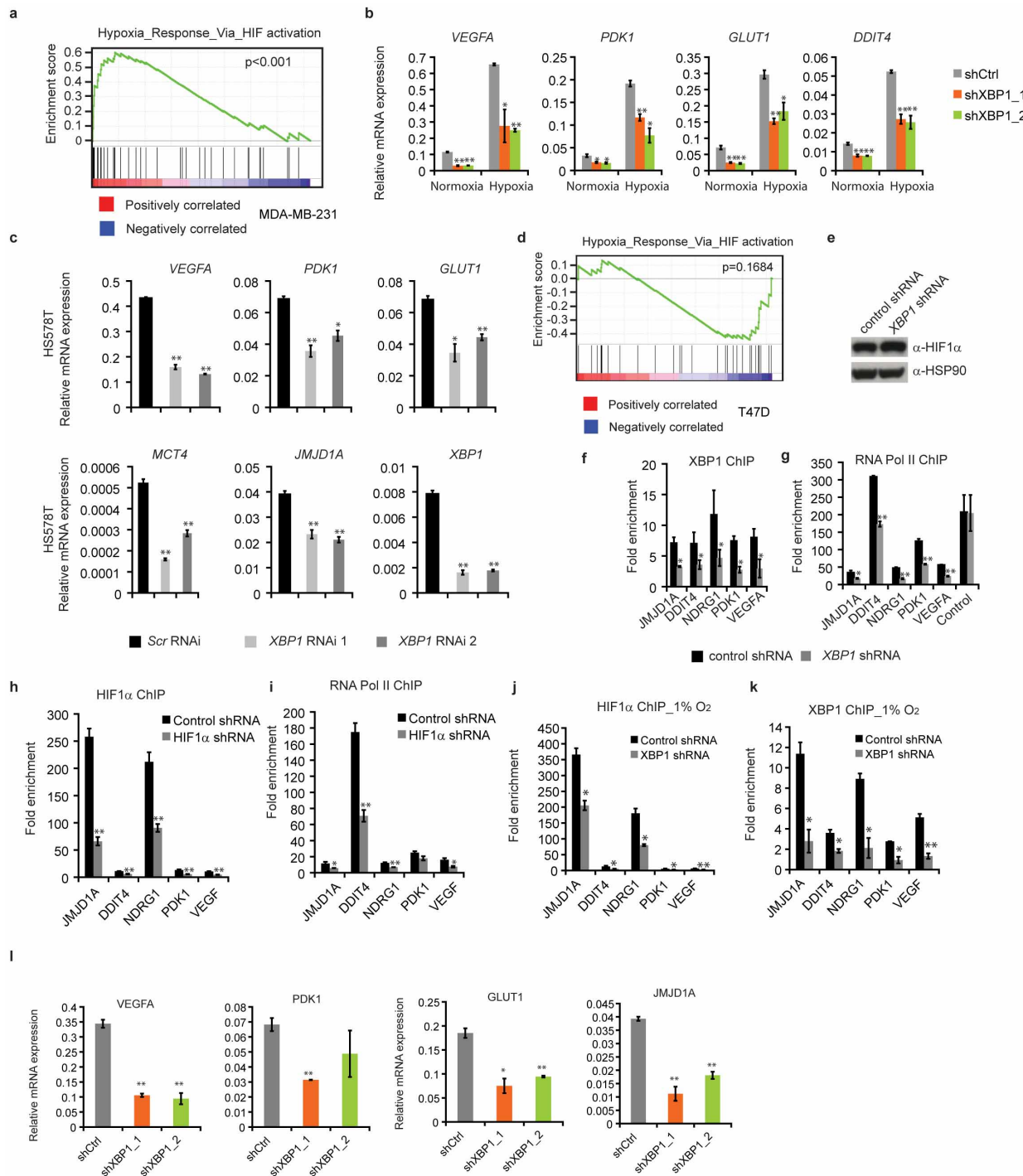
7.78×10^{-20} ; M231_HG, $< 1.08 \times 10^{-30}$; Hs578T_HG, $< 1.08 \times 10^{-30}$; T47D_HG, 6.14×10^{-6} . **h**, Flag-tagged HIF1α and XBP1s were co-expressed in 293T cells, and the cells were treated in 0.1% O₂ for 16 h. Co-immunoprecipitation was performed with M2 anti-Flag antibody. Western blot was carried out with anti-XBP1s antibody, anti-Flag antibody or anti-HIF1α antibody. Empty vector was used as control. **i**, Nuclear extracts from Hs578T cells treated with tunicamycin (1 μ g ml⁻¹, 6 h) in 0.1% O₂ (16 h) were subjected to co-immunoprecipitation with anti-HIF1α antibody or rabbit IgG. Western blot was carried out with anti-XBP1s antibody or anti-HIF1α antibody. **j**, HA-tagged HIF2α and XBP1s were co-expressed in 293T cells, and the cells were treated in 0.1% O₂ for 16 h. Co-immunoprecipitation was performed with anti-HA antibody. Western blot was carried out with anti-XBP1s antibody or anti-HA antibody. Empty vector was used as control. **k**, Localization of XBP1s and HIF1α in MDA-MB-231 cells. Western blotting analysis of XBP1s and HIF1α expression in cytosolic extracts and nuclear extracts of MDA-MB-231 cells cultured under 0.1% O₂ condition for 24 h. HSP90 and TBP were used as control. **l**, XBP1u is not expressed in MDA-MB-231 cells. Western blotting analysis of XBP1u in MDA-MB-231 cells untreated or treated with 1 μ M or 10 μ M MG132 for 4 h. HSP90 was used as loading control. **m**, Schematic diagram of full-length and truncated forms of XBP1s protein. **n**, A GST pull-down assay was performed using GST-tagged XBP1s proteins and 293T cell lysates overexpressing HA-tagged HIF1α. Western blotting was performed with an anti-HA antibody. Lower panel: Coomassie blue staining of GST-tagged different truncated forms of XBP1s proteins.



Extended Data Figure 5 | XBP1 and HIF1 α co-occupy HIF1 α targets.

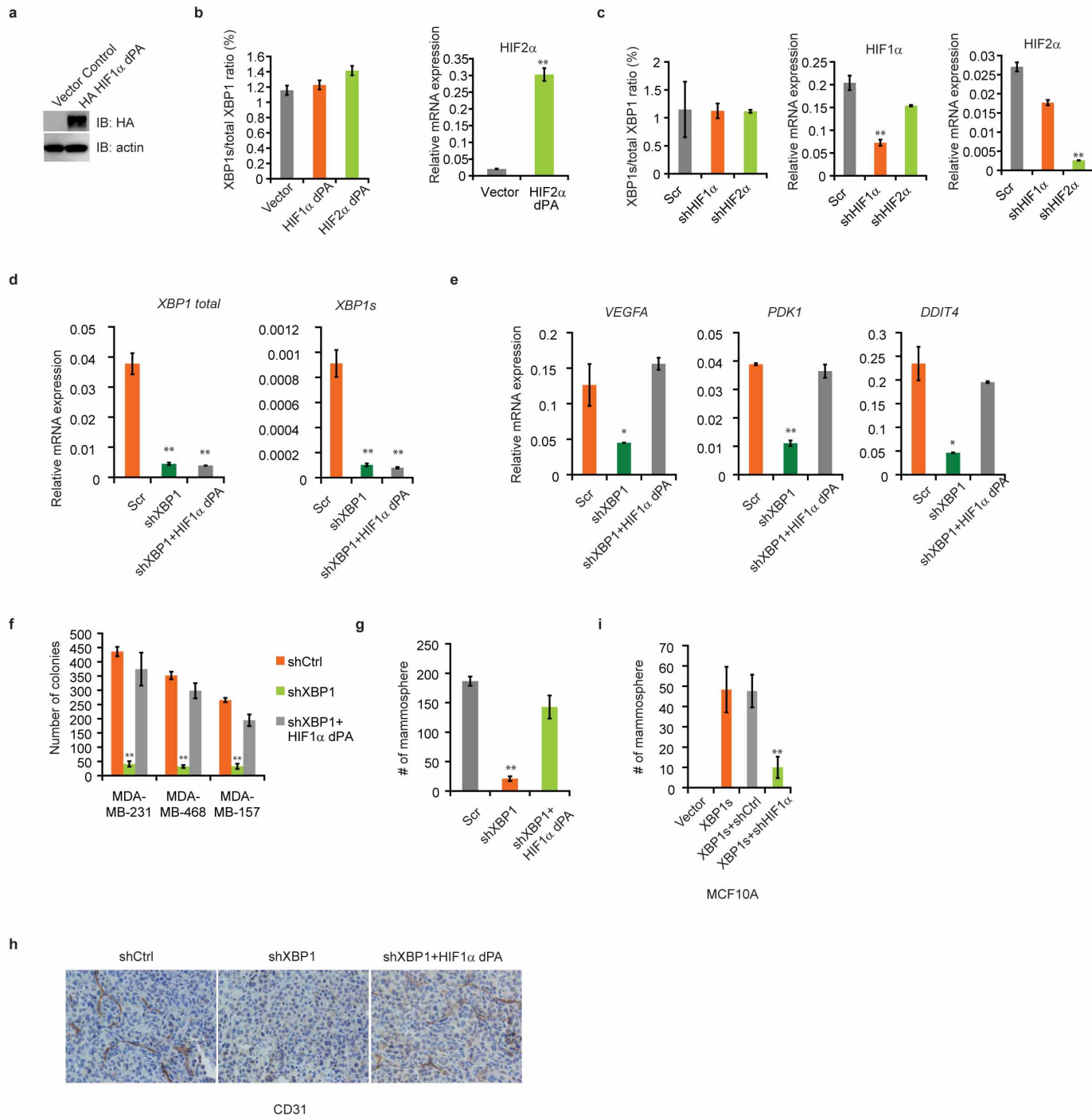
a, Track view of XBP1 ChIP-seq density profile (two biological replicates) on HIF1 α target genes. **b**, XBP1 and HIF1 α co-bind to *DDIT4*, *VEGFA* and *PDK1* promoters under hypoxic conditions. A ChIP assay was performed using anti-XBP1 or anti-HIF1 α antibody to detect enriched fragments. GST antibody was used as mock ChIP control. **c**, XBP1 and HIF1 α co-bind to *JMJD1A* and *JMJD2C* promoters under hypoxic conditions. Upper panel: schematic diagram of the primer locations across the *JMJD2C* or *JMJD1A* promoter. Grey boxes indicate exon. A ChIP assay was performed using anti-XBP1 polyclonal antibody or anti-HIF1 α polyclonal antibody to detect enriched fragments. Fold enrichment is the relative abundance of DNA fragments at the amplified region over a control amplified region. GST antibody was used as mock ChIP control. **d**, XBP1s and HIF1 α co-occupy *JMJD1A*, *DDIT4*, *NDRG1*, *PDK1* and *VEGFA* promoters. A ChIP-re-ChIP assay was performed using the anti-XBP1s antibody first (X). The eluants were then subjected to a second ChIP assay using an anti-HIF1 α antibody (XH) or a control IgG antibody (XC). All ChIP data (**b-d**) are shown as mean \pm s.d. of technical triplicates. Results

show a representative of two independent experiments. * $P < 0.05$; ** $P < 0.01$. **e**, HIF1 α , but not XBP1s, binds to a probe in *Twist* promoter in 293T cells. DNA pull-down assay was used to analyse the binding of XBP1s or HIF1 α on a probe in *Twist* promoter. The nuclear extracts of 293T cells overexpressing XBP1s or Flag-HIF1 α was incubated with the wild-type probe and immunoblot analysis was performed with anti-XBP1s or anti-Flag antibody. **f**, XBP1s binds to *Twist* promoter in MDA-MB-231 cells under 0.1% O₂. The nuclear extract of MDA-MB-231 cells cultured under 0.1% O₂ for 24 h was incubated with the wild-type or mutant probe (HIF1 α consensus sequence was mutated) and immunoblot analysis was performed with anti-XBP1s or anti-HIF1 α antibody. The lower panel shows the sequence of the probes used. **g**, 3 \times HRE reporter was co-transfected with XBP1s expression plasmid or empty vector into MDA-MB-231 cells and luciferase activity measured. Experiments were performed in triplicate and data are shown as mean \pm s.d. ** $P < 0.01$. **h**, RT-PCR analysis of XBP1 expression as in **g**. Data are shown as mean \pm s.d. of technical triplicates.



Extended Data Figure 6 | XBP1 regulates HIF1 α targets. **a**, Plot from GSEA showing enrichment of the HIF1 α -mediated hypoxia response pathway in XBP1-upregulated genes. **b**, Quantitative RT-PCR analysis of VEGFA, PDK1, GLUT1 and DDIT4 expression after knockdown of XBP1 in MDA-MB-231 under both normoxic or hypoxic conditions. **c**, Quantitative RT-PCR analysis of VEGFA, PDK1, GLUT1, MCT4, JMJD1A and XBP1 expression after knockdown of XBP1 in Hs578T cells treated with 0.1% O₂ for 24 h. Results are presented relative to β -actin expression. Experiments were performed in triplicate and data are shown as mean \pm s.d. *P < 0.05, **P < 0.01. **d**, Plot from GSEA showing no enrichment of the HIF1 α -mediated hypoxia response pathway in XBP1-regulated genes in T47D cells (P = 0.1684). **e–k**, Cooperative binding of XBP1 and HIF1 α on common targets. **e**, Immunoblotting analysis of control MDA-MB-231 cell lysates and XBP1 knockdown lysates (treated with 0.1% O₂ for 24 h) were performed using anti-HIF1 α or anti-HSP90 antibody. **f**, **g**, Chromatin extracts from control MDA-MB-231 cells or XBP1 knockdown MDA-MB-231 cells (treated with 0.1% O₂ for 24 h) were subjected to ChIP using anti-XBP1s antibody (**f**), or anti-RNA polymerase II antibody (**g**). The primers used to detect ChIP-enriched DNA were the peak pair of primers in JMJD1A, DDT4, NDRG1, PDK1 and VEGFA promoters (Supplementary Table 3). Primers in the β -actin region were used as control. **h**, **i**, Chromatin extracts from control MDA-MB-231 cells or HIF1 α knockdown MDA-MB-231 cells (treated with 0.1% O₂ for 24 h) were subjected to ChIP using anti-HIF1 α antibody (**h**), or anti-RNA polymerase II antibody (**i**). **j**, **k**, Chromatin extracts from control MDA-MB-231 cells or XBP1 knockdown MDA-MB-231 cells (treated with 1% O₂ for 24 h) were subjected to ChIP using anti-HIF1 α antibody (**j**), and anti-XBP1s antibody (**k**). All ChIP data (**f–k**) are shown as mean \pm s.d. of technical triplicates. Results show a representative of two independent experiments. *P < 0.05; **P < 0.01.

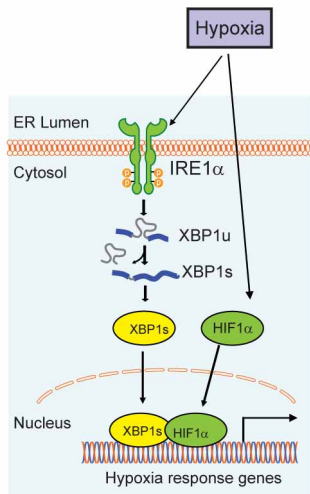
to ChIP using anti-XBP1s antibody (**f**), or anti-RNA polymerase II antibody (**g**). The primers used to detect ChIP-enriched DNA were the peak pair of primers in JMJD1A, DDT4, NDRG1, PDK1 and VEGFA promoters (Supplementary Table 3). Primers in the β -actin region were used as control. **h**, **i**, Chromatin extracts from control MDA-MB-231 cells or HIF1 α knockdown MDA-MB-231 cells (treated with 0.1% O₂ for 24 h) were subjected to ChIP using anti-HIF1 α antibody (**h**), or anti-RNA polymerase II antibody (**i**). **j**, **k**, Chromatin extracts from control MDA-MB-231 cells or XBP1 knockdown MDA-MB-231 cells (treated with 1% O₂ for 24 h) were subjected to ChIP using anti-HIF1 α antibody (**j**), and anti-XBP1s antibody (**k**). All ChIP data (**f–k**) are shown as mean \pm s.d. of technical triplicates. Results show a representative of two independent experiments. *P < 0.05; **P < 0.01. **l**, Quantitative RT-PCR analysis of VEGFA, PDK1, GLUT1 and JMJD1A after knockdown of XBP1 in MDA-MB-231 cells treated with 1% O₂ for 24 h. Results are presented relative to β -actin expression. Data are shown as mean \pm s.d. of technical triplicates. *P < 0.05, **P < 0.01.



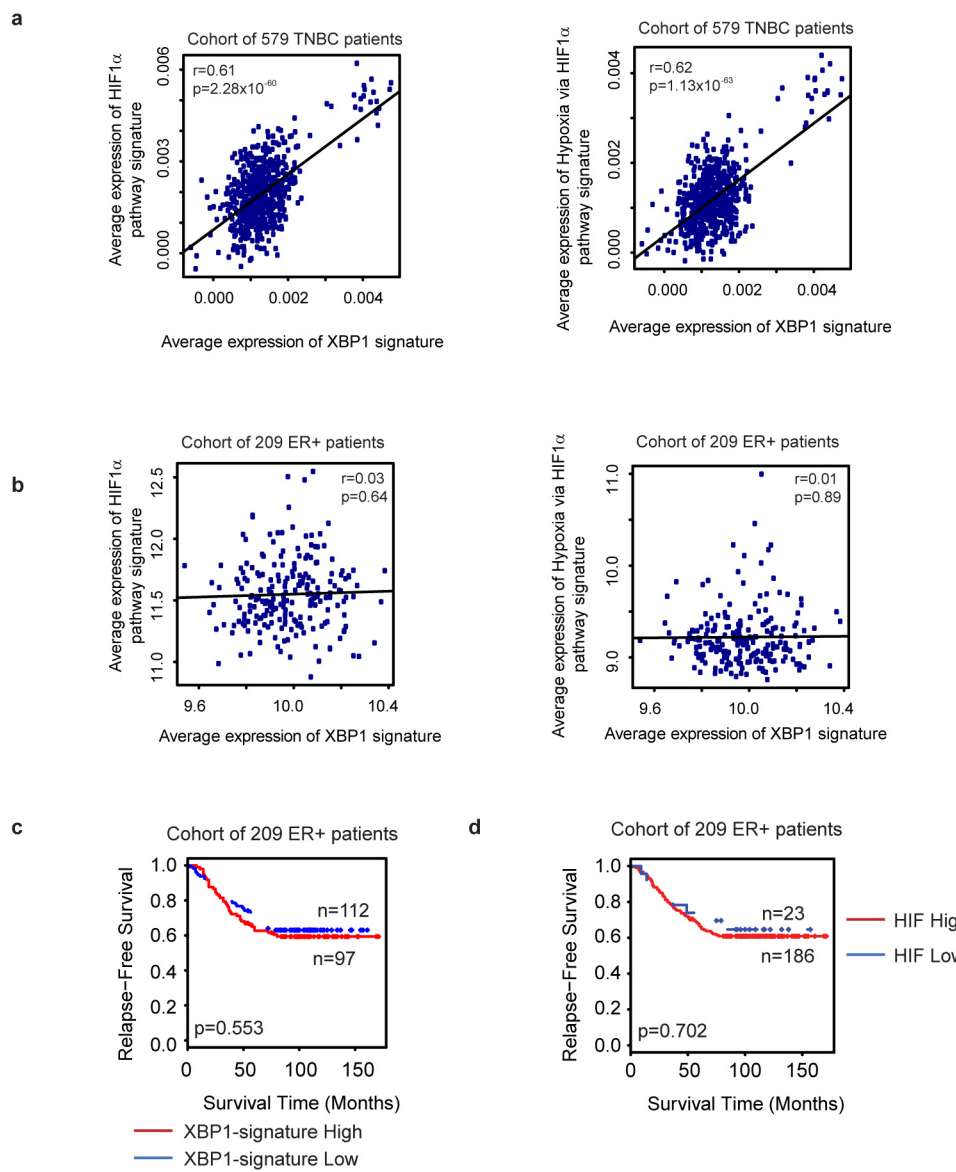
Extended Data Figure 7 | Overexpression of constitutively activated HIF1 α rescues XBP1 knockdown phenotype. **a**, Immunoblotting analysis of cell lysates of MDA-MB-231 cells infected with retrovirus encoding control vector or HA-HIF1 α dPA was performed using anti-HA or anti-actin antibody. **b**, XBP1 splicing is not affected by HIF1 α or HIF2 α activation. RT-PCR analysis of the ratio of XBP1s to total XBP1 in MDA-MB-231 cells expressing control vector, HA-HIF1 α dPA or HA-HIF2 α dPA. Expression of HA-HIF1 α dPA is shown in **a** and expression of HIF2 α is shown in the right panel. **c**, XBP1 splicing is not affected by HIF1 α or HIF2 α depletion. RT-PCR analysis of the ratio of XBP1s to total XBP1 in MDA-MB-231 cells infected with control, shHIF1 α or shHIF2 α lentivirus. Knockdown efficiency of HIF1 α or HIF2 α is shown in the middle and right panels. **d**, **e**, Expression of constitutively activated HIF1 α doesn't affect XBP1 expression (**d**), but restores HIF1 α targets expression (**e**). RT-PCR analysis of XBP1 total (**d**), XBP1s (**d**) and VEGFA, PDK1, DDIT4 (**e**) in control shRNA (shCtrl), XBP1 shRNA (shXBP1), or XBP1 shRNA plus constitutively activated HIF1 α (shXBP1 + HIF1 α dPA) infected MDA-MB-231 cells. Data (**b–e**) are shown as mean \pm s.d. of technical

triplicates. * $P < 0.05$, ** $P < 0.01$. **f**, Quantification of soft agar colony formation in control shRNA (shCtrl), XBP1 shRNA (shXBP1), or XBP1 shRNA plus constitutively activated HIF1 α (shXBP1 + HIF1 α dPA) infected MDA-MB-231, MDA-MB-468, or MDA-MB-157 cells. Experiments were performed in triplicate and data are shown as mean \pm s.d. ** $P < 0.01$.

g, Quantification of mammosphere formation in control shRNA (shCtrl), XBP1 shRNA (shXBP1), or XBP1 shRNA plus constitutively activated HIF1 α (shXBP1 + HIF1 α dPA) infected MDA-MB-231 cells. Experiments were performed in triplicate and data are shown as mean \pm s.d. ** $P < 0.01$. **h**, CD31 immunostaining of tumours formed by MDA-MB-231 cells infected with control shRNA (shCtrl), XBP1 shRNA (shXBP1) or XBP1 shRNA plus constitutively activated HIF1 α (shXBP1 + HIF1 α dPA). **i**, Silencing of HIF1 α inhibits the XBP1s-sustained mammosphere-forming ability. Quantification of mammosphere formation in MCF10A cells expressing control vector, XBP1s, XBP1s plus control shRNA or XBP1s plus HIF1 α shRNA. Experiments were performed in triplicate and data are shown as mean \pm s.d. ** $P < 0.01$.

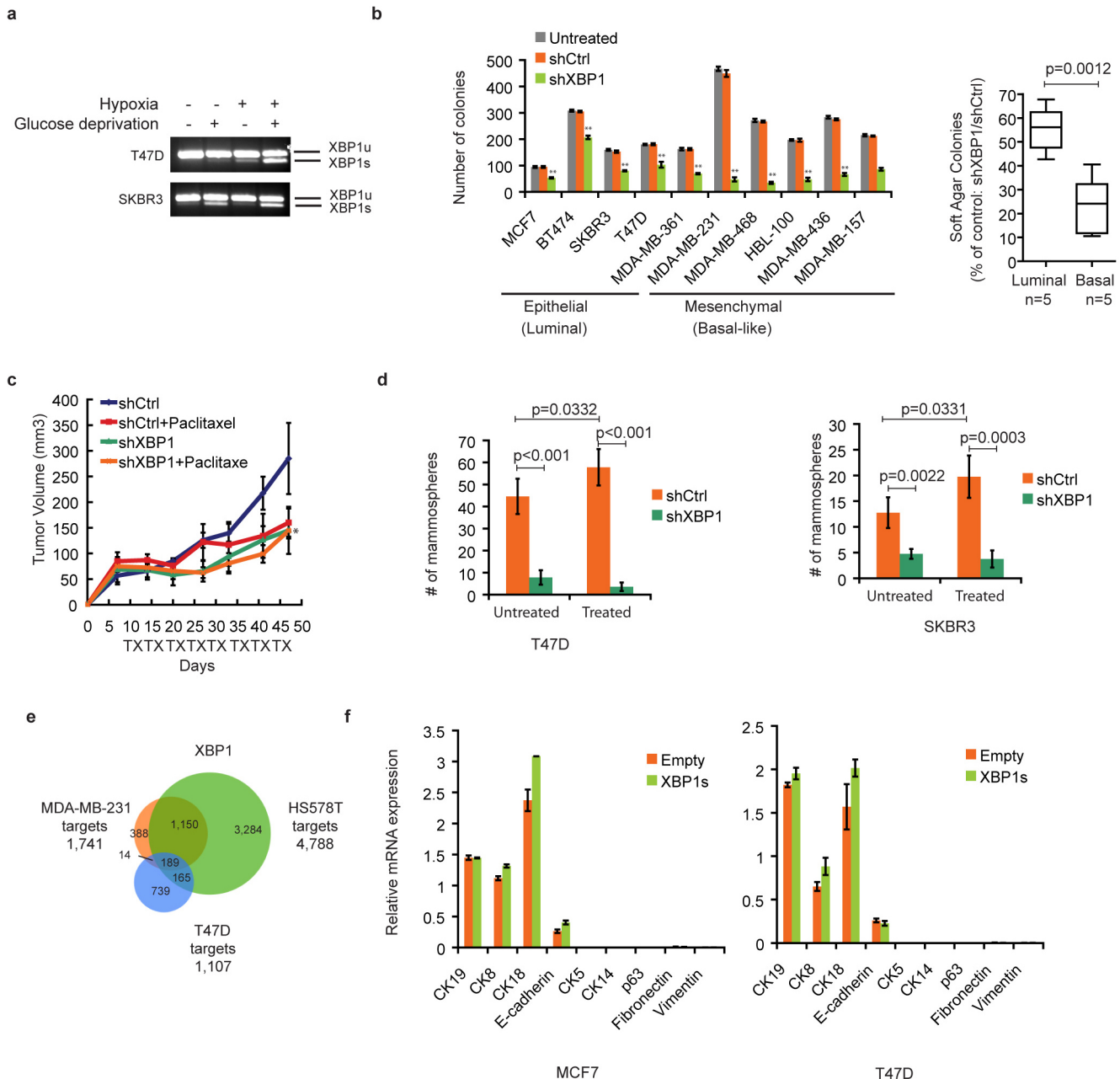


Extended Data Figure 8 | Schema depicting the interaction of XBP1 and HIF1 α in TNBC. XBP1 and HIF1 α cooperatively regulate HIF1 α targets in TNBC. In the setting of a tumour microenvironment, hypoxia further induces XBP1 activation; active XBP1s in turn interacts with HIF1 α to stimulate and augment the transactivation of HIF1 target genes that promote cancer progression.



Extended Data Figure 9 | Correlation of XBP1 with HIF1 α in patients with TNBC. **a, b,** Expression of XBP1 signature is highly correlated with two publicly available hypoxia-driven signatures in TNBC patients (**a**), but not in ER $^{+}$ breast cancer patients (**b**). The scatter plots of XBP1 and two publicly available HIF1 α signatures (left panel, HIF1 α pathway; right panel, hypoxia via HIF1 α pathway) across different tumours were drawn for TNBC (**a**) and ER $^{+}$

breast cancer patients (**b**), respectively. The corresponding Pearson's correlation coefficient (r) between XBP1 and HIF1 α signature is shown. **c, d,** Kaplan-Meier graphs demonstrating no significant association of the expression of the XBP1 signature (red line) (**c**) or HIF signature (**d**) with relapse-free survival in oestrogen-receptor-positive breast cancer patients. The log-rank test P values are shown.



Extended Data Figure 10 | Role of XBP1 in luminal breast cancer. **a**, XBP1 splicing is induced by hypoxia and glucose deprivation in luminal cancer cells. RT-PCR of XBP1 splicing in T47D and SKBR3 cells under different treatments for 24 h. XBP1u, unspliced XBP1; XBP1s, spliced XBP1. Hypoxia: 0.1% O₂. **b**, Left panel: quantification of soft agar colony formation in untreated and control shRNA or XBP1 shRNA infected breast cancer cells. Experiments were performed in triplicate and data are shown as mean \pm s.d. **P < 0.01. Right panel: effect of XBP1 depletion on soft agar colony formation in luminal versus basal cell lines. Percentages of soft agar colonies formed from cells infected with XBP1 shRNA lentivirus relative to the same cell line infected with shCtrl lentivirus (set as 100%) are presented. 5 cell lines in each group (as in left panel) and data are shown as mean \pm s.d. **c**, Tumour growth (mean \pm s.d.) of ZR-75-1 cells treated with control shRNA (n = 4), paclitaxel (20 mg kg⁻¹) + control shRNA (n = 4), XBP1 shRNA (n = 4) or paclitaxel + XBP1 shRNA (n = 3) in

nude mice. TX, treatment with shRNA or paclitaxel + shRNA. Asterisk denotes shXBP1-treated tumours significantly different from shCtrl-treated tumours; P < 0.05. **d**, Number of mammospheres per 1,000 cells generated by control shRNA or XBP1 shRNA-encoding lentivirus infected T47D or SKBR3 breast cancer cell lines cultured under normoxia or hypoxia and glucose deprivation conditions (treated). Experiments were performed in triplicate and data are shown as mean \pm s.d. **e**, Venn diagram showing the overlap between XBP1 targets in MDA-MB-231, Hs578T cells and T47D cells cultured under hypoxia and glucose deprivation conditions. **f**, XBP1s overexpression is not capable of converting a luminal phenotype to basal phenotype. RT-PCR analysis of luminal marker (CK8, CK18, CK19 and E-cadherin) and basal marker (CK5, CK14, p63, fibronectin and vimentin) expression in luminal breast cancer cells (MCF7 or T47D) infected with lentivirus encoding empty vector or XBP1s. Data are shown as mean \pm s.d. of technical triplicates.